High-order direct block support simulation and application at a gold mining complex

By

Joao Pedro de Carvalho

A thesis submitted to McGill University as a partial fulfilment of the requirements of the degree of Master of Engineering

Department of Mining and Materials Engineering

McGill University, Montreal

October, 2018

Acknowledgement

I want to thank to my thesis advisor Roussos Dimitrakopoulos for his countless pieces of critical advices. I have rarely seen someone so genuinely interested in helping and pushing students to deliver their best. I hope I have satisfied his expectations, and I am happy to have learned as much as I have with him.

I would like to thank to all the members of the COSMO lab that were present during my journey. Special thanks to Dr. Ilnur Minniakhmetov, for his immense help, explanations, and friendship; to Dr. Luis Montiel for always taking the time to help me with my doubts in mine planning; and my friend Ziad, for all the constructive discussions we have had, and for the countless English revisions he helped me with. I want to thank Adrien, Amina, Amir, Ashish, Christian, Cosmin, Daniel, Evan, Fernanda, Melanie, Lingqing, Ryan, Ray, Zachary and Zayneb all of whom were very present during my masters, as well to all past and new students. To Deborah Frankland, Barbara Hanley and Roselie Nardelli, for their unconditional help in all moments. To Prof. Claudio who has suggested me to come here in first place, thank you for all the encouragement.

Of course, this work would not be possible the support from our sponsors, who have my deepest gratitude. This work is funded by the National Science and Engineering Research Council of Canada, Natural Science and Engineering Research Council of Canada (NSERC) CRD Grant CRDPJ 500414-16, the COSMO mining industry consortium (AngloGold Ashanti, Barrick Gold, BHP, De Beers, IAMGOLD, Kinross, Newmont Mining and Vale), and NSERC Discovery Grant 239019.

Finally, I would like to thanks my parents Joao Bosco and Claudia, my sister Ana Cecilia for all their love, unconditional support, and encouragement. Their constant presence in my life made this work possible; it is not easy to be far from you all. My love Julia, thank you for being present in every moment of my life, listening to all my happy moments and frustrations, and always cheering me up. My brother Breno, even though you are far and we are not in touch every day, you are in my heart. To the TT group, I feel the energy of your prayers in my heart. To Phillipe and Pryscila, amazing friends that Montreal gave. Additionally, I would like to extend a special thanks to all my friends from Brazil and Montreal, sorry if I do not cite all of your names, but it would require at least another thesis of this size to express my gratitude.

Contribution of authors

This section states the contribution of the co-author of the papers that comprise the present work. The author of this thesis is the primary author of all the work presented herein. The work was completed with the supervision and advice of his advisor Prof. Roussos Dimitrakopoulos, who is also the co-author on the two papers, comprising this thesis. Dr. Ilnur Minniakhmetov is an additional co-author of the paper presented in Chapter - 2.

Chapter - 2: de Carvalho JP, Dimitrakopoulos R, Minniakhmetov I (2018). High-order block support spatial simulation and application at a gold deposit. (Submitted) Mathematical Geosciences.

Chapter - 3: de Carvalho JP, Dimitrakopoulos R (2018). Effects of high-order simulations on the simultaneous stochastic optimization of mining complexes. (to be submitted)

Abstract

Over recent years, new methods have developed the mining production schedule stochastic optimization into a framework that includes, in one mathematical formulation, all the components of a mining complex and optimizes it simultaneously. A mining complex is a set of operations that integrate all aspects in a mineral value chain, starting from the materials extracted from the ground culminating with its transformations into a final product delivered to the mineral market. The framework diverges from past methods that optimize each operation of the mining complex separately, which do not benefit from the coexisting harmony between connected processors. Core inputs of this all-inclusive optimization are the geostatistical simulations quantifying variability and uncertainty of relevant attributes in a given mineral deposit. To date, the state-of-the-art simulation methods can reproduce complex, non-linear geometries and multi-point connectivity of extreme values. However, the generated realizations are performed at the point-support, much like the drillhole data, which requires a post-processing step to generate block-support orebody models, as needed to represent the mineral deposit due to engineering purposes. For example, a multimillion block model requires discretization of the magnitude of hundreds of millions of nodes to simulate. This configuration presents computational challenges in generating, handling and post-processing such a massive model. The thesis proposes an approach that extends the high-order simulation framework to perform realizations directly at the block-support scale and explores an application of such a method when used as input to the simultaneous optimization of a mining complex. Thereby, illustrating the benefits of coupling simulations that capture a more realistic connectivity of high-grades with the simultaneous stochastic optimization framework.

The first part of this thesis presents the high-order simulation method that generates realizations directly at the block support conditioned to the available data at point support scale. Following the sequential simulation paradigm, the method estimates, at each block location, the cross-support joint probability density function using Legendre-like splines as the set of basis functions needed. The previously simulated blocks are added to the set of conditioning data, which initially contains the available drillhole data at the point support. A spatial template, defined by the configuration of the block to be simulated and related conditioning values in both support scales, is used to infer additional high-order statistics from a training image. First, the method is tested

in a controlled environment, and the simulated realizations show consistent results reproducing major structures and high-order relations of data. Second, the method is used to simulate a gold deposit, and its efficiency is demonstrated by reproducing spatial statistics up to a fourth-order, coinciding with the ones present in the available drillhole data. The running time of generating one realization with the proposed approach is reduced by a factor of 5 when compared to the point-support version of the algorithm.

The second part of the thesis presents a case study where the simulations of the gold deposit mentioned above are incorporated into the simultaneous optimization of a gold mining complex. The resulting life-of-mine (LOM) production schedule yields 5 to 16% higher net present value when compared to the case, where the same mining complex is optimized, but the deposit is modelled through a traditional simulation method based on two-points statistics (sequential Gaussian simulation). The comparison shows that incorporating simulations with more realistic connectivities of high-grade blocks, through the use of high-order direct block simulations, into the optimization results in a more informed LOM production schedule. The sequence of extraction is visually driven towards areas where the high grades are more connected, and this smarter extraction strategy leads to the extraction of less waste and the production of more ounces earlier in the LOM. This shows that the optimization can capitalize on the better understanding of the connectivity of high-grades.

Résumé

Au cours des dernières années, de nouvelles méthodes d'optimisation mathématique stochastique permettant d'optimiser simultanément un vaste ensemble de décisions devant être prises lors la planification de la production d'un complexe minier ont été développées. Un complexe minier implique un ensemble d'opérations qui constituent une chaîne d'approvisionnement minière, en commençant par l'extraction du minerai du gisement jusqu'à sa transformation finale en produit mis sur le marché. Cette optimisation simultanée se différencie des approches antérieures où les diverses opérations du complexe minier sont optimisées indépendamment les unes des autres, ce qui ne permet pas de tirer profit des fortes dépendances entre les différents processus. Les données d'entrée essentielles à cette optimisation simultanée sont des simulations géostatistiques qui quantifient la variabilité et l'incertitude des attributs d'un gisement de minerai donné. Quoique les méthodes de simulation les plus avancées permettent de reproduire des géométries complexes et non-linéaires ainsi que la connectivité multipoints des valeurs extrêmes, il demeure néanmoins que les réalisations obtenus avec ces méthodes sont générées à l'échelle des points, tout comme les données de forage, ce qui requiert une étape de post-traitement pour générer les modèles de gisement à l'échelle des blocs. Cette étape de post-traitement est nécessaire pour représenter le gisement pour des fins d'opérations d'ingénierie. Ainsi, un modèle à plusieurs millions de blocs nécessite une discrétisation de l'ordre de plusieurs centaines de millions de points à simuler. Cela représente un défi computationnel de taille en termes de génération, manipulation et post-traitement de ces modèles. Ce mémoire propose une approche qui génère des réalisations directement à l'échelle des blocs dans un contexte de simulation d'ordre supérieur. L'application des résultats de cette approche comme données d'entrée pour l'optimisation simultanée d'un complexe minier est aussi présentée. Cette application illustre les avantages associés au couplage de simulations, qui représentent de manière plus réaliste la connectivité des fortes teneurs, avec un système d'optimisation stochastique simultanée.

La première partie de ce mémoire présente la méthode de simulation d'ordre supérieur proposée permettant de générer des réalisations directement à l'échelle des blocs avec les données conditionnelles disponibles à l'échelle des points. Suivant le paradigme de la simulation séquentielle, la méthode estime, pour chaque emplacement de bloc, la fonction de densité de probabilité commune à support croisé en utilisant des splines de type Legendre comme ensemble

de fonctions de base nécessaires. Les blocs précédemment simulés sont ajoutés à l'ensemble des données conditionnelles, qui contient initialement les données de forage disponibles à l'échelle du point. Un motif spatial, défini par la configuration du bloc à simuler et les données conditionnelles correspondantes, est utilisé pour déterminer des statistiques d'ordre supérieur additionnelles venant d'une image d'entraînement (training image). La méthode proposée est d'abord testée dans un environnement contrôlé. Les résultats de ces tests démontrent que les réalisations simulées présentent des résultats consistants reproduisant les structures majeures ainsi que les relations d'ordre supérieur des données. Dans un second temps, la méthode est utilisée pour simuler un gisement d'or. Cette étude confirme l'efficacité et la capacité de la méthode à reproduire les statistiques spatiales jusqu'au 4^{e} ordre, tout en étant conforme à ces mêmes statistiques venant des données de forage. Le temps de calcul nécessaire pour générer une réalisation avec l'approche proposée est réduit d'un facteur de 5 comparativement à la version de l'algorithme considérant l'échelle du point.

La deuxième partie du mémoire présente une étude de cas où les simulations obtenues via l'approche décrite ci-haut sont utilisées comme données d'entrée pour l'optimisation simultanée d'un complexe minier. Les résultats de cette optimisation indiquent qu'une valeur présente nette de 5 à 16% plus élevée est obtenue comparativement à une optimisation prenant comme données d'entrée des simulations générées avec une méthode traditionnelle basée sur des statistiques du 2^{e} ordre (simulation Gaussienne séquentielle). La comparaison montre aussi qu'utiliser des simulations présentant des connectivités de blocs à fortes teneurs plus réalistes permet d'obtenir une planification de production mieux informée. La séquence d'extraction suit visuellement les régions où les fortes teneurs sont connectées et cette extraction plus intelligente entraîne moins d'extraction de stérile ainsi que la production de plus d'onces de métal plus tôt durant la période d'exploitation de la mine. Cela montre que l'optimisation peut capitaliser sur une meilleure compréhension de la connectivité des fortes teneurs.

Table of contents

List of tables

List of figures

List of terms

CPU	Central processing unit
cdf	Cumulative distribution function
cpdf	Conditional probability density function
DBSIM	Direct block simulation
ENESIM	Extended normal equations simulation
GPU	Graphics processing unit
GSGS	Generalized sequential Gaussian simulation
HOSIM	High-order simulation
jpdf	Joint probability density function
LU	Lower upper decomposition
LOM	Life-of-mine
MAF	Minimum/maximum autocorrelation factors
MIP	Mixed integer programming
MPS	Multiple-point statistics
NPV	Net present value
PFS	Probability field simulation
RAM	Random access memory
RF	Random field
SNESIM	Single normal equation simulation
SIS	Sequential indicator simulation
SIP	Stochastic integer programming
SGS	Sequential Gaussian simulation
TI	Training image

Chapter - 1

Literature Review

1.1 Introduction

A mining complex can be seen as a mineral value chain where in-situ materials are extracted from the ground and flow through different processing streams until they are transformed into sellable products and delivered to the mineral market (Pimentel et al. 2010; Montiel and Dimitrakopoulos 2015; Goodfellow and Dimitrakopoulos 2016). Current industry practice in long-term mine planning attempts to maximize the net present value (NPV) by optimizing separately various aspects of the mineral value chain, including optimal mine design, cut-off grades, stockpile decisions, processing streams and transportation systems. New research has shifted away from this step-wise optimization process towards the state-of-the-art simultaneous stochastic optimization of mining complex framework (Montiel and Dimitrakopoulos 2013, 2015, 2018; Farmer 2016; Goodfellow and Dimitrakopoulos 2016, 2017; Montiel et al. 2016; Saliba and Dimitrakopoulos 2017; Del Castillo 2018). This unified approach can incorporate several mines, stockpiles, waste dumps, processing facilities, operational modes, transportation mechanisms and many other aspects complex in one single non-linear mathematical formulation. This simultaneous optimization has the potential to unveil hidden and profitable synergies between different components that traditional approaches cannot capture.

The goal of the value chain optimization is to provide the mineral market with metals and other products where the supply of materials extracted from the mines are characterized by the uncertainty and variability of the geological attributes. This supply uncertainty is incorporated into the framework as a group of simulated orebody models with their respective relevant attributes. This associated uncertainty, quantity and quality of pertinent mineral deposit attributes can be assessed through transfer functions, meaning representing mathematically the transformations in consideration, and geostatistical simulations, which generates multiple equiprobable scenarios of the attributes of interest, such as grades, densities, material types, hardness, and others geo-metallurgical properties. The material extracted from the orebody flows through many different processes in the mining complex, propagating the uncertainty to all operations in the mining complex, which culminates in financial risk. In addition to the

uncertainty, geologic variability is also an inherent aspect of mineral deposits; these aspects related to the supply uncertainty combined are the major source of risk in a mining operation and the leading cause of failure in delivering expected production targets (Ravenscroft 1992; Dowd 1994, 1997; Vallée 2000; Dimitrakopoulos et al. 2002a; Godoy 2003; Dimitrakopoulos 2011). Incorporating the uncertainty and variability associated with the supply of materials into the mining complex framework enables risk-managing mine planning schedules with better blending decisions, more informed destination decisions, amongst others.

This chapter reviews the technical literature related to orebody modelling through the use of geostatistical simulations, and their use in the simultaneous stochastic optimization of mining complexes. Section 1.2 covers most advanced methods in mineral deposit modelling, based on multi-point statistics and high-order spatial statistics, limitations of traditional second-order simulation framework, as well as the efforts in efficiently generating stochastic realizations of a given mineral deposit. Section 1.3 discusses the impact different simulations frameworks have an activity modelled by a transfer function. Section 1.4 examines the technical literature related to the optimization frameworks connecting different components of a mining complex and the most recent state-of-the-art simultaneous optimization of mining complexes. Section 1.5 provides the goal and objectives of this thesis, and Section 1.6 presents the thesis outline.

1.2 Mineral deposit modelling

Modelling of mineral deposits for resource and reserve assessment in mining planning consists of discretizing space into a three-dimensional block model and assigning values of spatially distributed attributes of interest; examples of such are metal content (grade), density, hardness, amongst others. The material from the mineral deposit is considered to be the material supply for the mining complex. The uncertainty material supply is due to the exploration drilling and sampling pattern obtained at non-continuous and scattered locations. The core sample diameter has a magnitude of centimetres, which is considered to be at “quasi-point” (or point-support) size. On the other hand, engineering applications in geosciences model the mineral deposits into mining blocks, representing the engineering requirements necessary to extract. A small block size overestimates the selectivity that realistic size equipment has, and a large block size incurs dilution in the model, underestimating the selectivity.

Geostatistics is a branch of statistics that concerns with the quantification of the uncertainty and quality of spatially distributed attributes in a mineral deposit, that takes into account this difference in support sizes (volume-variance effect). It is based on the concept of random field (RF) processes, where the goal is to model the distribution of the RF $Z(u_i)$ at the location u_i, which is indexed in the domain D delimiting the boundaries of the mineral deposit ($u_i \in D$). Outcomes of $Z(u_i)$ are denoted by $z_i = z(u_i)$ and can represent attributes of interest, such as grades, density, hardness, material types, and other geological property. The $Z(u_i)$ distribution is conditional to nearby sample values denoted as $d_n = \{Z(x_j), j = i,\ldots,n\}$ where n represents the number of neighbouring values contribution to building the conditional probability density function (pdf) in u_i.

Since a very small percentage of the mineral deposit is sampled, there are two approaches to deal with the assessment at unsampled locations, through estimation or simulations, which differ from the fundaments. Estimations interpolate the unsampled locations through a weighted average of the data nearby (David 1977; Journel and Huijbregts 1978; Isaaks and Srivastava 1989; Goovaerts 1997). The drawback is that all estimation methods result in a smoothing of the data distribution and they prevent the assessment of the uncertainty. The smoothing effect is characterized by an overestimation of low values and an underestimation of high values (Goovaerts 1997). The consequence of this smoothing is the misrepresentation of tonnages and grades, and when used as input in the mining planning context, it becomes the leading cause of not meeting expected targets (Ravenscroft 1992; Dowd 1994, 1997; Vallée 2000; Dimitrakopoulos et al. 2002a; Godoy 2003; Dimitrakopoulos 2011).

Geostatistical simulations are Monte Carlo simulations, where the orebody is modelled as a random field, and each simulation can be drawn from a conditional probability density function. The simulations aim to reproduce the spatial statistics obtained from data, and consequently the deposit variability. Performing multiple Monte Carlo simulations generate stochastic scenarios enabling the uncertainty assessment of related random field and the generation of risk analysis profiles for the task where stochastic simulations are used.

The sequential simulation approach is one of the most applied simulations strategies in the industry. It relies on the decomposition of a multivariate probability density function of the related random field into products of univariate posterior distributions (Johnson 1987; Journel and Alabert 1989; Journel 1994; Goovaerts 1997; Dimitrakopoulos and Luo 2004), as shown in Eq. 1.

$$f_{\mathbf{Z}}\left(u_1,\ldots,u_n;z_1,\ldots,z_n\middle|\Lambda_0\right)=f_{Z_1}\left(u_1;z_1\middle|\Lambda_0\right)*\ldots*f_{Z_n}\left(u_n;z_n\middle|\Lambda_{n-1}\right)=\prod_{i=1}^{n}f_{Z_i}\left(u_i;z_i\middle|\Lambda_{i-1}\right) \quad (1)$$

where $\mathbf{Z}=\left(Z_1,\cdots,Z_n\right)$ .The $\Lambda_0=d_n$ denotes the set containing the available exploration data $\Lambda_0=d_n$. At every time a node $\boldsymbol{u}_i$ is simulated, its value is incorporated into the set of conditioning data for the next node to be simulated $\Lambda_i=\left\{u_i;z_i,\Lambda_{i-1}\right\}$. Note that this decomposition is not unique. Thus a random path visits all the $\boldsymbol{u}_i$ locations in order to obtain one simulated scenario.

The following steps summarize the sequential simulation framework:

a) Generate a random path visiting all nodes to be simulated.
b) At every node $\boldsymbol{u}_i$, estimate the conditional pdf $f_{Z_i}\left(u_i;z_i\middle|\Lambda_{i-1}\right)$.
    a. From the probability distribution obtained in b), draw a random realization z_i and updated the set of conditioning values to Λ_i.
c) Repeat all the steps for additional realizations.

1.2.1 Traditional stochastic simulation methods

Under the geostatistical simulation approaches, the sequential Gaussian simulation (SGS) is the most commonly used method in mining industry applications (Isaaks 1990; Journel 1994; Goovaerts 1997). In this method, the RF is assumed multi-Gaussian, i.e. each of the probability density function $f_{Z_i}\left(u_i;z_i\middle|\Lambda_{i-1}\right)$ to be estimated becomes Gaussian. This assumption facilitates the generation of the conditional pdf since it only requires defining the mean and variance at every location. First, the approach requires to transform the initial data to the Gaussian space and to define a global variograms model for the RF. The variogram is responsible for measuring the

average spatial dissimilarity given a certain distance in a specific direction. Then at every unsampled location, the algorithm solves the kriging equations to generate a conditional mean $m\left(Z\left(x_i\right)|\Lambda_{i-1}\right)$ and variance $var\left(Z\left(x_i\right)|\Lambda_{i-1}\right)$ from $f_{Z_i}\left(u_i;z_i|\Lambda_{i-1}\right)$ by solving kriging equations at every node. These two parameters are enough to construct a Gaussian pdf; thus the method samples a value from this generated distribution through Monte Carlo and incorporates it into the grid to be used as conditioning for the next location's simulation. After the simulation of all the nodes, the values are back-transformed from the Gaussian space to the original data space to match the original histogram of the data.

Since SGS is based on the definition of a variogram model and only calculates cumulants – combination of moment statistical parameters – spatial statistics of first and second orders, namely mean and variance respectively, it belongs to the class of methods based on second-order. The major limitation of these methods is that second-order spatial statistics are not sufficient to describe complex and non-linear natural phenomena. Journel (2007) shows a simple example, shown in Fig. 1.1, where different geologic patterns display very similar variograms. Obtaining samples in such a way that the values are the same regardless of the true mineralization and modelling one variogram from this sample set is not sufficient to discriminate between these possible candidates. The resulting simulation does not have the means to distinguish between these different connectivity patterns. Therefore it cannot generate more complex and non-linear geologic structures.

Methods based on second-order statistic requiring the Gaussian assumption over the conditional distribution functions indirectly assume that the multiple-point spatial statistics and multiple-point connectivity are given by the related algorithm and not by the data or other sources of information (Remy et al. 2009). The methods in this context are responsible for maximizing the spatial disorder beyond the variogram model. Entropy herein is a concept related to the spatial disorder, e.g. how the extreme values are structured. Strings of low or high values connected, channels, curvilinear structures, depositional veins, beddings and others are examples of low entropy and characteristics of mineral deposits. High entropic methods generate realizations where geologic structures are unjustifiedly disconnected, and "salt-and-pepper" structures can be observed (Journel and Deutsch 1993). In the light of the above, high entropy has substantial consequences when the goal is to evaluate the response of the simulated realizations in a context

governed by non-linear transfer functions, such as effective permeability, flow simulation in aquifers or oil reservoirs and optimization of mine designs. Gaussian-based simulation approaches, in turn, are maximal entropy methods, which are not desired characteristics in geostatistical simulations.

This effect has consequences in petroleum reservoir and aquifers due to the misinterpretation in flow modelling (Journel and Alabert 1989; Journel and Deutsch 1993; Gómez-Hernández and Wen 1998; Renard and Allard 2013). Journel and Deutsch (1993) present a waterflood simulation example using three different geostatistical simulation methods, where time at which the watercut reaches 90% is investigated. Results show that the reference time value, obtained from a reference image, is outside the range provided by SGS realizations; while the range of values provided by other methods, that reproduce better the connectivity of extreme values, can capture this reference value. Journel and Alabert (1989) show a comparison where a Gaussian-based method is not able to reproduce as well as a non-gaussian method the connectivity of a sandstone model, marked by a strong connectivity of low values, and the connectivity map is shown in Fig. 1.2. This entropy property can also impact mining operations since the continuity of mineralization of high-grades drives the optimization of production schedules.

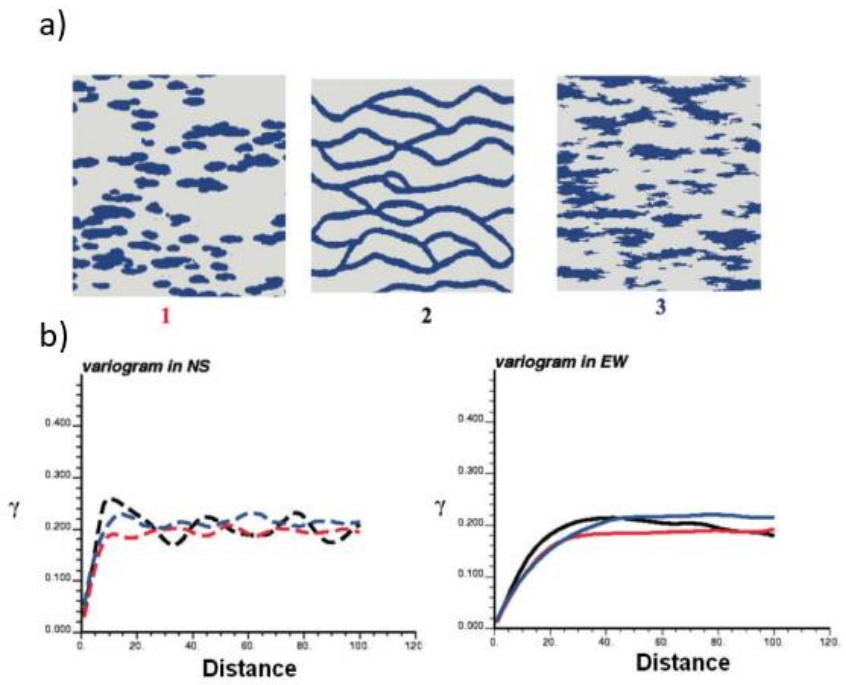

Figure 1.1 – Example of the limitations of second-order statistics (Journel 2007). a) different spatial patterns and their similar variograms in b).

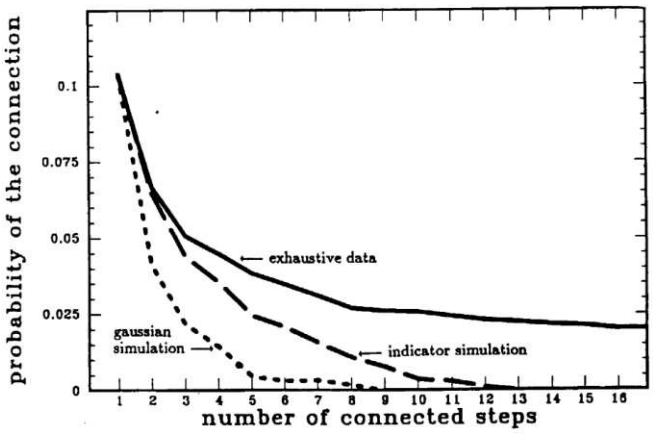

Figure 1.2 – Experimental connectivity in the N57° direction of the exhaustive dataset, and SGS and SIS realizations of the Borea sandstone dataset (Journel and Alabert 1989).

Sequential indicator simulation (SIS) (Alabert 1987; Goovaerts 1997) is an alternative to Gaussian-based methods that do not require a Gaussian transformation of the initial data. Instead, the ranges of values are discretized in categories. For the continuous case, the non-parametric conditional cumulative distribution function (cdf) is estimated through successive indicator kriging for each pre-defined category. At each step, the probability of not surpassing each category is calculated, while for the discrete case, the order of classes does not matter. Once the conditional cdf is built, a uniform value $[0,1]$ is drawn, and the category associated with the value is the simulated class. SIS improves the high-grade connectivity of the realizations compared to SGS because it does not require a Gaussian distribution of values and it can incorporate spatial statistics for many indicators. The method improves the connectivity of extreme values because a variogram these categories are calculated directly, which provides more information to the generated realization. As oppose to SGS which model only one average variogram model for all the deposit, limiting the incorporation of spatial statistics. The practice of this SIS simulation requires more calibration as it involves a definition of one variogram model for each category. Additionally, the approximation of the tails of skewed conditional distributions is hard to control (Rossi and Deutsch 2014). Although can describe more complex spatial features than SGS, the method still carry the limitations of second-order methods.

Other classes of simulation methods including turning bands (Journel 1974; David 1977; Journel and Huijbregts 1978), probability field simulation (Froidevaux 1992; Goovaerts 1997), simulated annealing (Deutsch and Cockerham 1994; Goovaerts 1997), direct sequential simulation (Soares 2001) are alternatives to simulate an orebody model. They all carry major limitations of either relying only on a variogram model and Gaussian transformation of data.

1.2.2 Direct block-support simulation methods

Mineral deposits models usually comprise between hundreds of thousands up to millions of mining blocks. Such an extensive model requires an efficient framework to generate simulations. The samples obtained from drillholes are collected at point-support, meaning the framework must provide means to change the support from point to blocks. The traditional approach to deal with this difference in support sizes consists of subdividing the blocks into several internal nodes, which can represent the point support. The simulation is then performed at this new denser grid, and later these internal nodes are post-processed averaged into a block support value.

The block assessment from point values is shown in Eq. 2, where the RF $Z_V(v)$ represents the block support assessment at the location v from $Z_p(u_j)$ point support assessments.

$$Z_V(v) = \frac{1}{|V|} \int_{u_j \in v} Z_P(u_j)\, du_j. \tag{2}$$

This traditional way of converting point simulations to block models can be limiting when dealing with large mineral deposits. Considering a multimillion block model of a mineral deposit, the necessary point support discretization would result in billions of nodes to simulate. Such computation can be very inefficient and demanding. Additionally, generating several simulations at this fine scale requires a massive amount of memory space for calculation, storage and data handling. Under these circumstances, a direct block assessment is highly desired, where past efforts focused on improving the efficiency of simulation methods, which is a major requirement for the industry.

Upon the observation that adjacent nodes share the same neighbourhood, Dimitrakopoulos and Luo (2004) enhance the computational efficiency of Gaussian-based simulations with the

"generalized sequential Gaussian simulation" (GSGS) algorithm. The approach requires the definition of group sizes, which means how many nodes are going to be simulated together according to LU equations (Davis 1987). A random path visits each group, and then each node within a group is randomly placed in the LU matrix. If all nodes are considered into one single group, the method becomes analogous to the LU simulation method, if there is only one node per group it corresponds to SGS. Benndorf and Dimitrakopoulos (2007) document a study where GSGS can be up to 20 times faster than SGS on the same deposit; however, it still requires a posterior re-blocking since realizations are outputted at the point support.

A significant extension of sequential Gaussian simulations is provided by the direct block simulation (DBSIM) method (Godoy 2003). Following a random path visiting each node, the approach discretizes the block into several internal nodes, and simulates the nodes within, using the LU approach. The difference is that in the simulation of each node, the method calculates the covariance between points and points, blocks and points, and blocks and blocks. After the simulation of nodes within the block, the values are averaged into a single block value, and only this last one is kept as conditioning for the next block to be simulated. DBSIM approach is faster than GSGS, but most important the direct block support method reduces the storage requirement considerably (Benndorf and Dimitrakopoulos 2007). Also, no re-blocking post-process is required to generate mining blocks. Boucher and Dimitrakopoulos (2009) propose an extension for the block support that can simulate multiple correlated variables. Before the simulation, a vector random function is orthogonalized by the minimum/maximum autocorrelation factors (MAF) (Switzer and Green 1984; Desbarats and Dimitrakopoulos 2000). These de-correlated variables are simulated independently in the same context as DBSIM. The difference is that once the nodes within the block are simulated two processes occur in parallel. First, the nodes are averaged for conditioning to the next block to be simulated. Second, the point values are back-transformed to the Gaussian space, followed by a transformation to the data space, so they can finally be averaged into a block value in the original space. An example of the framework is shown in Fig. 1.3.

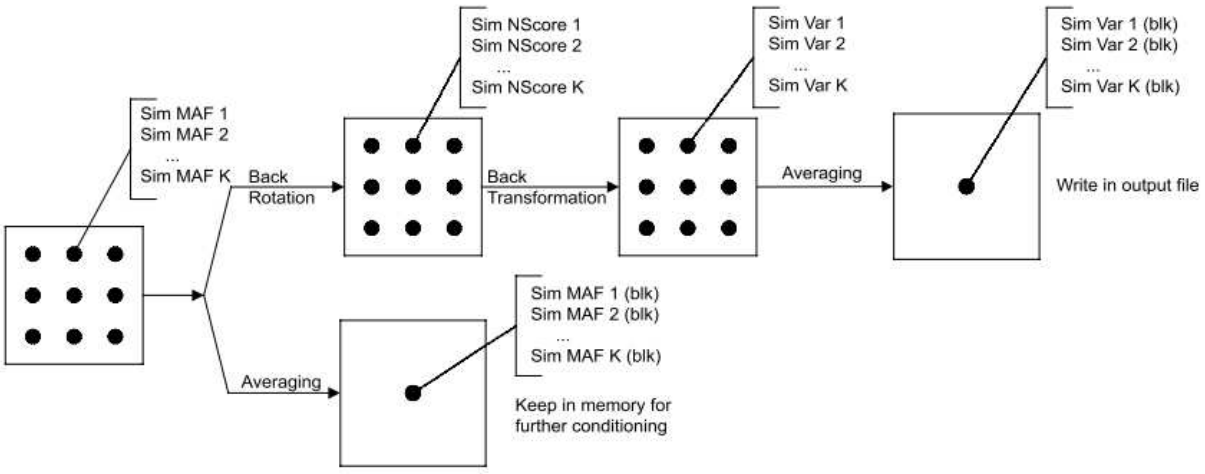

Figure 1.3 – Framework for the block support simulation of multivariate correlated elements (Boucher and Dimitrakopoulos 2009).

Emery (2009) proposes a simulation method that uses an explicit change of the support model and directly simulates at block support, without discretizing the blocks into several nodes, reducing CPU running time required. The proposed model is entirely defined by a point support Gaussian transformation function, a change of support coefficient and the block support semivariograms. One of the limitations of the approach is related to introduction of an additional coefficient that must be defined by the user. This coefficient joint to the Gaussian transformation at point-support are used to derive the Gaussian transformation at the block support. This framework can enhance the entropy aspect of the realizations and the separated data-conditioning step can reduce the efficiency of the approach in generating conditional realizations.

Although efficient, all of the methods mentioned above share common limitations, they require data transformation, assume the conditional distribution is Gaussian, related spatial statistics is limited to two-point spatial statistics, and some methods require a more strict assumption on the stationarity of related RF.

1.2.3 New developments in stochastic simulations

When the distributions are assumed to be Gaussian, only mean and covariance (variogram) are enough to define the whole distribution since all high-order moments become zero. However, geologic phenomena in geoscience are not Gaussian, and more statistics are necessary to be incorporated. To overcome the limitations of second-order methods, a more advanced class of

methods founded on the multiple-point statistics (MPS) has been leveraged by the petroleum industry since the 90s (Guardiano and Srivastava 1993; Strebelle 2002; Remy et al. 2009; Mariethoz and Caers 2014). The methods herein replace the random field model by a framework that extracts patterns from a training image (TI). The TI is a geological analogue of the variable in consideration, which is assumed to be representative of the spatial data distribution and acts as a supplemental pattern database for the original exploration data. A data-event is a spatial arrangement of values and can be represented by a set of conditioning values nearby surrounding the central node, as shown in Fig. 1.4. The whole spatial configuration of this data-event and the central node is a template used as a basis to find similar patterns in the TI. In this setting, the spatial statistics between multiple points altogether can be incorporated into the framework enabling the stochastic realizations to reproduce complex and curvilinear geologic patterns.

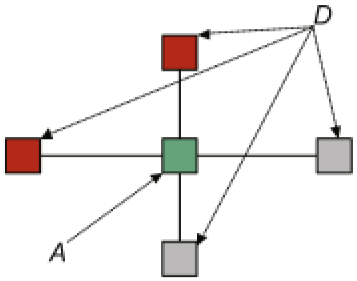

Figure 1.4 – Example of a template, with central node A and data event D (Goodfellow et al. 2012).

1.2.3.1 Multiple-point statistical methods

Among the MPS methods, research mostly focuses on two main branches: pixel-based and pattern-based simulations. The first one consists in simulating each node at a time, while the latter focus on pasting a whole pattern (set of values) from the training image directly at the simulation grid. Pioneer work is credited to Guardiano and Srivastava (1993) by proposing the MPS framework and "ENESIM" (extended normal equations) algorithm and focus on simulating one node at a time. The approach scans the TI searching for a similar data-event that is given by the original data plus some previously simulated nodes. The patterns obtained generate a conditional probability which is used to simulate a value to the node. The additional information incorporated into the algorithm is precisely the multi-point covariance that is obtained from the TI. According to Guardiano and Srivastava (1993), consider K categories $\{z_k, k = 1, \cdots, K\}$ and

let A_k be an indicator variable assuming a unitary value if the random variable $Z(u_i)$ receives the outcome $z(u_i) = z_k$ at the location u_i.

$$A_k = \begin{cases} 1, & if \quad Z(u_i) = z_k \\ 0 & otherwise \end{cases} \tag{3}$$

Similarly, let D be a binary random variable indicating the occurrence of the data event d_n. The conditional probability at the node u_i to be assigned the category z_k is given by

$$f_{Z_k}(u_i; z_k | d_n) = P(A_k = 1 | D = 1) = \frac{P(A_k = 1, D = 1)}{P(D = 1)} \tag{4}$$

The frequency of categories and data events found in the TI generate the above probability. Once these frequencies are obtained, a Monte Carlo simulation assigns the value relative to the category and includes it in the grid as conditioning. The algorithm requires searching the TI at every iteration, which is very computationally demanding. Strebelle (2002) improves this framework with the "SNESIM" algorithm. Given a categorical dataset, the approach assumes a fixed template, which allows scanning the TI only once to store the frequency of patterns in a search tree. It enables the conditional probabilities to be rapidly computed from this data structure. The conditional probability for each node is built finding exact replicates of the data-event given the template generated and counting the frequency of each category from the TI to be represented in that configuration. When the exact match is not found, some of the conditioning data are dropped relaxing the conditioning requirements of finding a replicate, with the cost of worse conditioning at that location. The running time is considerably improved, but the memory requirements grow exponentially with the size of the template and the number of categories assumed. In general, the template size is kept small, and this could prevent the reproduction of large-scale features, but the implementation of multiple grids attenuates it. An alternative is to use a hierarchical approach (Maharaja 2004), where the categories to be simulated are nested, and the simulation is performed in stages. The disadvantage is related to that not all spatial interactions between different categories can be acquired.

Under the SNESIM framework, Boucher (2009) proposes to partition the training image into smaller images. Each subset is responsible for generating a search tree itself. The partitions are

obtained applying spatial filters that discriminate different patterns based on geometric configuration. The idea is to use a vector of smaller search trees instead of a global one, which speeds up the algorithm. Straubhaar et al. (2011) replace the use of a search tree with lists data structure to store the multiple-point patterns. This replacement reduces the RAM required to the simulation, and additional lists can be used to incorporate secondary information. A list increases linearly with template size, while the tree grows exponentially. This data structure enables to use larger templates at a smaller computation cost; consequently, a more complex reproduction of geologic patterns is possible to be obtained. Searching patterns in the list can be less efficient, but this operation can be parallelized. Huang et al. (2013) implement GPU computation for the SNESIM algorithm using the search tree data structures showing a speedup of 15 times compared to the original version of the algorithm. Strebelle and Cavelius (2014) attempt to alleviate the memory and the running time requirements on SNESIM method by proposing a new multiple-grid approach, which includes intermediary sub-grid that reduces the need for larger templates. The sub-grid structure provides a similar reach of large-scale structures, with a smaller template. Although it increases the number of search trees, the one-time cost of creating a new search tree is compensated by smaller trees; thus finding probabilities at each node becomes faster. Additionally, they propose a new data template configuration that preferentially includes previously simulated nodes and closest ones, which is based on the simulation of the past sub-grids. The authors claim that this also reduces the need to get bigger templates and that this strategy is sufficient to provide multiple point connectivity.

Mariethoz et al. (2010) extend the initial ENESIM algorithm to a direct sampling method that reduces memory usage considerably by instead creating a TI database for the generation of the conditional distribution, it samples a pixel straight from the TI. Given a conditional data event at a particular node, replicates from the TI are sampled directly, and the similarity between the data event and the replicate is calculated. If this distance is smaller than a threshold, the central node of the replicate is pasted in the simulation grid. The sampled value is chosen randomly but still conditional to the data. This approach is mathematically equivalent to computing a conditional cdf at every node based on the patterns from the TI and drawing a sample from it.

By avoiding the explicit definition of a random field, MPS methods become flexible with room for applications in many different fields. However, limitations of the above methods are related to the lack of mathematical formality, concentrating on the extraction of patterns from the TI

instead of deriving conditional distributions based on high-order statistics. Thus, the statistics of the exploration data cannot be guaranteed. This TI-driven characteristic is particularly problematic in the mining context, an environment often marked by a wealth of exploration data. Past studies have shown conflicts between the statistics of the generated realization and exploration data (Osterholt and Dimitrakopoulos 2007; Goodfellow et al. 2012). The spatial statistics of the simulation respect the statistics present in the TI but do not necessarily consider the ones from the drillholes, which is the reality of a given deposit. When the realizations over reproduce patterns from the TI, a question that arises is how much the TI is representative and how to obtain it.

In the context of the equally TI-driven pattern-based MPS methods, Arpat and Caers (2007) propose an approach that pastes directly in the simulation grid a whole multi-pixel pattern configuration extracted from the TI. The first step consists of building a TI database according to a fixed template. Later, the method chooses the most similar pattern according to a distance measurement, instead of drawing from a probability distribution. The method allows modifying previously simulated nodes if the new pattern to be pasted overwrites it. As a drawback, the algorithm lacks in mathematical formulation, and the focus is preferably on the reproduction of patterns from the TI rather than deriving a conditional distribution function based on the spatial statistics of the data. Additionally, scanning the whole database at every iteration is computationally expensive.

An alternative to the computing limitation of scanning the full TI discussed above is the FILTERSIM algorithm (Zhang et al. 2006). The method first scans the training image with a template of fixed size and classifies the patterns present in a filter space. Few linear filters are used to reduce the dimension of the pattern itself, and training patterns that are similar are grouped under an average pattern. These patterns are grouped in bins according to a similarity measure or score values. During the simulation, the bin that best matches the conditioning data event is chosen, and a pattern is selected from this bin and pasted in the simulation grid. This configuration provides a more structured ranking of patterns, which reduces the RAM demand and avoids scanning the database extensively to find similar patterns. These pattern-based simulation approaches tend to reproduce local multi-point statistics by allowing global patterns from the TI to be reproduced, enhancing the approaches' TI-dependency and generating simulations even more TI-driven. The size of the template is a user-defined parameter and has a

major influence in the realizations. The structure to classify the patterns also plays an important role. It is necessary to balance between meaningful patterns and a not extremely large number of bins storing the patterns. Wu et al. (2008) replace the pixel-wise distance by the score-based distance calculated in the filter space.

Chatterjee et al. (2012) propose a pattern based simulation applying wavelet decomposition to the patterns scanned from the TI. From the weights obtained with the decomposition, the algorithms apply a clustering algorithm to classify the patterns. The method compares the L2 norm with the data event and the pattern representative of the generated cluster. In which for the categorical case the best match is and for the continuous case it is chosen at random a pattern from the chosen cluster. Mustapha et al. (2014) propose a framework that encodes the TI pattern database into a one-dimensional space, which improves the running time for the pattern classification and its comparison with the data event. Rezaee et al. (2013) combine the advantages of the pixel-based "direct sampling" method (Mariethoz et al. 2010) with pattern-based simulations eliminating the need to build a training image pattern database.

In general, pattern-based simulations carry all the major limitations of pixel-based MPS approaches, with the addition that the conditioning process is more challenging to obtain appropriately. When the template size is larger than the spacing between original data, pasting the whole piece of pattern would either overwrite some data or be somehow the cause of mismatch.

There are other multiple-point simulation alternative methods to the above mentioned, such as the ones based on the simulated annealing approach (Kirkpatrick et al. 1983; Geman and Geman 1984; Goovaerts 1997; Deutsch and Wen 2000). A training image can be used to provide frequencies of the patterns to be reproduced in the simulation. These frequencies are set to be targets in the objective function of the simulated annealing algorithm, and an iterative process attempts to minimize the mismatch between those two (Ortiz and Peredo 2010; Peredo and Ortiz 2011). The running time of the approach can be enhanced with parallel computing (Peredo and Ortiz 2011). In addition to the typical limitations of MPS methods, they introduce additional user-defined parameters, which are not trivial to tune and can be time-consuming

1.2.3.2 High-order simulation methods

As an alternative to the above, and a natural extension of the random field model, a high-order simulation (HOSIM) framework is proposed by Dimitrakopoulos et al. (2010). They introduce the high-order spatial cumulants which are used to describe complex geological configurations and high-order connectivity. Cumulants are a combination of moment statistical parameters and can be seen as the extension of the well-known mean and covariance function, first and second order cumulants respectively. Recalling the random field $Z(u_i)$ at location u_i, denoted as Z_i for simplicity of notation, Eqs. 5 and 6 show how the moments can be calculated and the relation between cumulants $c_{i_1 \cdots i_n}$ and moments $m_{j_1 \cdots j_n}$

$$Mom\left(Z_1^{i_1} \cdots Z_n^{i_m}\right) = m_{i_0 \cdots i_n} = E\left[Z_1^{i_1} \cdots Z_n^{i_n}\right] = \int_D Z_1^{i_1} \cdots Z_n^{i_n} f_Z(z_1, \cdots, z_n) dz \tag{5}$$

$$\begin{aligned} Cum\left(Z_1^{i_1} \cdots Z_n^{i_n}\right) = c_{i_1 \cdots i_n} = & \sum_{j_1=0}^{i_1} \cdots \sum_{j_{n-1}=0}^{i_{n-1}} \sum_{j_n=0}^{i_n - 1} \binom{i_1}{j_1} \cdots \binom{i_{n-1}}{j_{n-1}} \binom{i_n - 1}{j_n} \\ & \times c_{i_1 - j_1, \cdots, i_{n-1} - j_{n-1}, i_n - j_n} m_{j_1 \cdots j_n} \end{aligned} \tag{6}$$

Mustapha and Dimitrakopoulos (2010) propose a method that estimates the conditional density function through Legendre polynomials $P_j(z)$ (Lebedev 1965) and high-order spatial cumulants. This estimation makes no assumptions regarding the initial distribution of data values. It is important to note that, by construction, the cumulants of order k, carry information of lower order cumulants, as shown in Eq. 6. By calculating the high-order cumulants, information about the low order cumulants are implicitly incorporated, as the low-order spatial statistics can be easily seen in the initial dataset; therefore they are also reproduced by the final realizations.

Recalling the conditional probability decomposition according to the sequential simulation framework presented in section 1.2 , with n locations to simulate:

$$\begin{aligned} f_{\mathbf{Z}}(u_1, \ldots, u_n; z_1, \ldots, z_n | \Lambda_0) = & f_{Z_1}(u_1; z_1 | \Lambda_0) * \ldots * f_{Z_n}(u_n; z_n | \Lambda_{n-1}) = \\ & \prod_{i=1}^{n} f_{Z_i}(u_i; z_i | \Lambda_{i-1}) \end{aligned} \tag{7}$$

where $\mathbf{Z} = (Z_1, \cdots, Z_n)$; Λ_0 is the initial conditioning data and Λ_{i-1} is the set with conditioning data and previously simulated nodes. Without loss of generality, take u_1 as the node to be simulated. The conditional probability distribution $f_{Z_1}(z_1|\Lambda_0)$ at this location according to Bayes' rule can be decomposed in

$$f_{Z_1}(z_1|\Lambda_0) = \frac{1}{\int_D f_{\mathbf{Z}}(z_1, z_2, \cdots, z_n) dz_0} f_{\mathbf{Z}}(z_1, z_2, \cdots, z_n). \tag{8}$$

The joint distribution from above can be approximated by Legendre Polynomials $P_j(z)$ and the respective Legendre coefficients $L_{i_0, i_1, \cdots, i_N}$:

$$f_Z(z_1, z_2, \cdots, z_n) \approx \sum_{i_1=0}^{\infty} \sum_{i_2=0}^{\infty} \cdots \sum_{i_N=0}^{\infty} \overline{L}_{i_1, i_2, \cdots, i_N} \overline{P}_{i_1}(z_1) \tag{9}$$

where

$$\overline{L}_{i_1, i_2, \cdots, i_n} = L_{i_1, i_2, \cdots, i_n} \overline{P}_{i_2}(z_2) \cdots \overline{P}_{i_n}(z_n) \tag{10}$$

and

$$\overline{P}_j(z) = \frac{\sqrt{2j+1}}{\sqrt{2}} P_j(z). \tag{11}$$

The Legendre coefficients are responsible for capturing the high-order spatial statistics, and are function of the cumulants of degree $i_0, i_1, \cdots, i_N$, and by the orthogonal property of the Legendre polynomials, they can be experimentally obtained according to

$$\begin{aligned} L_{i_1, i_2, \cdots, i_n} &= \int_D \overline{P}_{i_1}(z_1) \overline{P}_{i_2}(z_2) \cdots \overline{P}_{i_n}(z_n) f_Z(z_1, z_2, \cdots, z_n) \\ &= E\left[\overline{P}_{i_1}(z_1) \overline{P}_{i_2}(z_2) \cdots \overline{P}_{i_n}(z_n) \right]. \end{aligned} \tag{12}$$

Note that the node to be simulated u_1 and the conditioning values at location $u_2, \cdots, u_n$ form a spatial template. The template is used then to search the simulation grid and TI to search for

replicates, which are used as input for calculating the high-order Legendre coefficients experimentally as in Eq.12. This strategy differs from MPS methods that assume a fixed and arbitrary template.

The high-order simulation method (Mustapha and Dimitrakopoulos 2010a, 2011) can be summarized according to the following steps:

a) Scan the training image and sample data and store the spatial cumulants in a global tree.
b) Define a random path visiting all nodes to be simulated.
c) At each node, define the spatial template with the node to be simulated and its neighbours. Obtain the replicates from the global tree defined in a). Calculate the Legendre coefficients as in Eq. 12.
d) Approximate the conditional cdf according to Eqs. 8 and 9.
e) Draw a random value from the derive distribution, and add this value to the grid so it can be used as conditioning to the next node.
f) Repeat (b)-(e) until all nodes are simulated.
g) Repeat (b)-(f) for additional realizations.

One of the disadvantages of the above lie in the expensive computational time required to derive all high-order cumulants at every node. To save time without compromising the quality of the realizations, Mustapha and Dimitrakopoulos (2011) propose removing the calculation of cumulants with small contributions to the estimation of the cpdf. The drawback is that the polynomial approximation can be very unstable, especially at the endpoints of the data domain. Minniakhmetov et al. (2018) replace the Legendre polynomials with the Legendre-like splines (Wei et al. 2013). The authors use the m first Legendre polynomials and discretize the approximation domain in several knots, which are responsible for defining the condition of smoothness of the splines. These knots associated with the initial Legendre polynomials are the basis to create a space with all necessary orthogonal splines. The idea is to replace high-degree and instable polynomials with several ones of lower degree defined in delimited intervals. The substitution provides to the conditional distributions a more stable approximation due to the power of representation of the splines, as shown in Figure 1.5.

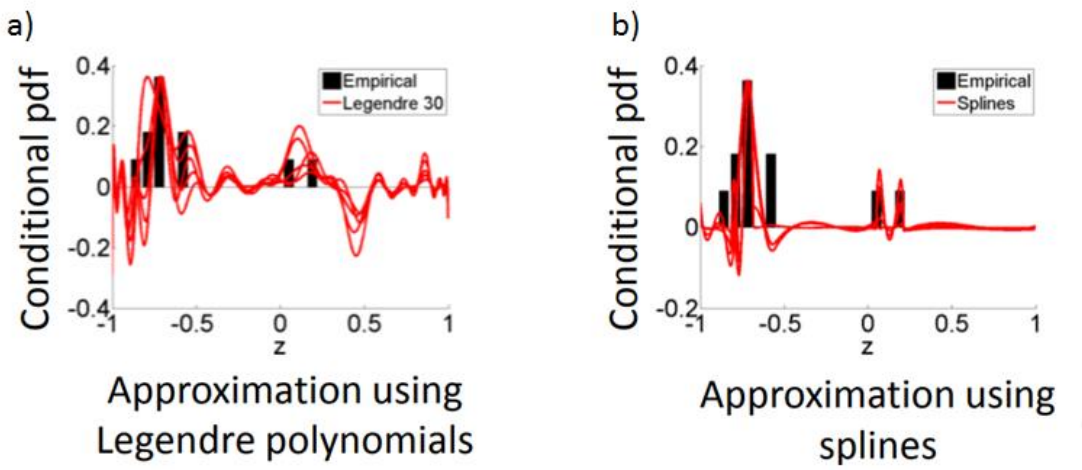

Figure 1.5 – Example of empirical approximation using a) Legendre polynomials of degree 30 and b) splines. Provided by Minniakhmetov et al. (2018)

Dealing with multivariate elements, Minniakhmetov and Dimitrakopoulos (2017a) present a method to decorrelate variables based on spatial high-order statistics using a diagonal domination condition approach. For independent variables, the high-order cumulants are diagonal. Thus, the approach transforms the vector of random variables maximizing the diagonal independence of high-order cumulants. The framework then simulates these variables independently and back transforms the values in order to maintain the high-order relationship. Addressing one of the limitations of high-order and MPS method, the dependency of training images, Minniakhmetov and Dimitrakopoulos (2017b) propose a new data-driven high-order simulation method for categorical values. The high-order spatial moments are entirely obtained from the available data, and no training image is needed. They make use of boundary conditions on the calculation of moments. Taking, for instance, a third-order spatial indicator moment which is a function of two lags, when one of the lags goes to 0, this indicator moment becomes the second-order moment. On the other hand, when one lag is very large, the two moments become independent. For intermediate lags, the moments are approximated with B-splines functions.

Yao et al. (2018) simplify the calculation of high-order spatial cumulants and the polynomial approximation in a unified function. The approach does not require any explicit calculation of cumulants or moments. The simplicity ends up speeding up the simulations at no cost in the reproduction of complex patterns. High-order simulations are a powerful tool to model non-Gaussian attributes with complex geologic patterns; however, these state-of-the-art methods are

still performed at the point scale. A deposit with millions of blocks would require the simulation of billions of nodes, which is still computationally cumbersome. It asks for a framework that can simulate directly at the scale of blocks, which is one of the goals of this thesis.

1.3 Effects of simulations on transfer functions

Stochastic simulations are a powerful tool to model uncertainty and variability of a geologic variable. They are also used to quantify the uncertainty in transfer functions, which are mathematical models that map the response of attributes in a specific context, such as mine production scheduling, flow simulation, and many others. Mapping the uncertainty of the outputs is vital in a mining context since most of transformations and operations in a mining complex can be mathematically modelled as a transfer function. Therefore, this is another aspect that captures the interest of the current research. This section reviews past studies that highlight the benefits of simulations methods in the optimization of mining-related transfer functions. The drawbacks of using traditional estimation methods instead stochastic simulations is already a well-studied topic (Ravenscroft 1992; Dowd 1994; Dimitrakopoulos et al. 2002b). Still, it is worth mentioning here that this is related to the fact that an average input does not result in an average output when dealing with non-linear transfer functions, which reinforces the need to use stochastic simulations in an optimization context.

Dimitrakopoulos (1996) presents a short example of the use of stochastic simulations on a characterization of reservoir production forecasts. The study highlights the misleading forecast obtained with non-stochastic methods resulting in about $80 million less revenue than expected. Conversely, stochastic simulations were able to predict the recovery efficiency to be much closer to the obtained in reality. The author points out that the criterion for generating reservoir descriptions and decision (which is extended to mineral deposits as well) must be based on the mapping of the uncertainty of the responses; as each stochastic realization generates one response when applied to a transfer function.

Qureshi and Dimitrakopoulos (2005) study the impact of three different simulations methods on three transfer functions that are analogues to some present in the mining context. From an extensive and known dataset, the author samples values from it to generate stochastic realizations of SGS, SIS and probability field simulation (PFS) (Goovaerts 1997). A set of 100 realizations of each simulation method is pushed through the following transfer functions: minimum cost

network flow, threshold proportion and geometric mean. Finally, the performance of all frameworks is compared to the extensive dataset and assessed regarding precision and bias. Overall, the sequential simulations, SGS and SIS, have a similar performance in mapping the uncertainty of the response of uncertainty, both incorporating the main features necessary of the geologic domain.

Dimitrakopoulos and Godoy (2014) present a study where the same three simulation methods mentioned above are applied in a grade control optimization context. In short-term planning, grade control is an operation where the blasted material is flagged as ore or waste according to economic valuation, traditionally based on an economic cut-off. Usually, blastholes samples are collected to provide guidance in this ore/waste selection. The most critical aspect of grade control is the misclassification, which can result in future financial losses. Also note that this is a non-linear transfer function, as the impact of sending ore to waste is not the same as sending waste to the processing facility. The comparison concludes that SIS is the method that returns the highest profit. The result is related to high cut-off applied and the maximal entropy property of Gaussian-based simulations. The maximal entropy provides the realizations with a randomized dispersion of high-grades, which understates the connectivity of the high values. Conversely, the SIS method does not require a Gaussian transformation and can incorporate spatial statistics at many different thresholds, which results in more realistic connectivity of high-grades.

Albor and Dimitrakopoulos (2009) and Montiel and Dimitrakopoulos (2017) study the influence of the number of simulations necessary to generate a LOM production schedule that is stable under geologic uncertainty. Albor and Dimitrakopoulos (2009) perform a sensitivity analysis by optimizing the mine design inputting a different number of simulations between 2 and 20. Montiel and Dimitrakopoulos (2017) present a similar study but in the context of simultaneous optimization of a mining complex. Both studies conclude that a number between 10 and 15 simulations are enough to generate stable solutions. This is explained by the support-scale effect, where each period of a production schedule is composed by thousands of mining blocks, this represents a scale of magnitude very different from the scale of individual mining blocks; therefore there is no significant additional information passed to the optimizer after this point (number of simulations).

The studies presented in this section highlight the need to understand the mapping the uncertainty of the response of transfer functions. However, they do not discuss how the simulation method can influence the LOM production schedule. Additionally, it is worth investigating the benefits of realizations generated by a framework able to provide more informed geologic models, such as HOSIM methods. High-order simulations are the state-of-the-art in modelling connectivity of non-Gaussian variables with complex and non-linear geometries. Therefore, in the context of a mining complex, there is room to explore the potential profit in modelling more realistically the connectivity of high-grades, which are the driver of the LOM production schedule optimization.

1.4 Long-term mine planning optimization

The utmost goal of a strategic long-term mine plan is the determination of when to extract and where to send each portion of the geological block model obeying a series of technical constraints in order to maximize the economic value of the project. Most common strategies to solve such a task rely on mathematical modelling based on Mixed Integer Programming (MIP) (Urbaez and Dagdelen 1999). The MIP approaches represent the orebody as a three-dimensional block model, where the most relevant attributes are described, examples of such are tonnages, grades, hardness, density, and other metallurgical properties.

1.4.1 Optimizing the components of the value chain

A mining complex is a supply chain approach that integrates all operations from resources to mineral markets (Whittle 2010; Montiel and Dimitrakopoulos 2015; Goodfellow and Dimitrakopoulos 2017). It can comprise multiple mines (open-pit or underground), stockpiles, waste dumps, tailing facilities, processors, operational modes and transportation systems (Pimentel et al. 2010). The simultaneous optimization of a mining complex aims to optimize extraction sequences, destination policies, processing stream decisions, transportation alternatives altogether in one single mathematical model. This framework can be seen as a series of transfer functions that account for the transformations of in-situ material throughout the value chain, which can include plenty of non-linear interactions such as cut-off grade optimization, non-additive geo-metallurgical responses, blending, non-linear recovery curves, stockpiling, capital expenditure decisions and many others.

Industry practice usually manages all the operations within the mining complex through the disconnected optimization of several components, which leads to suboptimal solutions. More effective efforts to incorporate several mineral value chain components start in the 1990s. Hoerger et al. (1999) provide an overview of an in-house MIP optimizer for the expansive gold complex operations in Nevada. The optimization comprises multiple pits, several material types and different destinations whose material could flow through the value chain. The model is extremely large, and some simplifications are assumed to decrease the number of decision variables. Regardless of the computational limits, it is important to note the goal of optimizing many components together and profit from the existing synergies between the upstream and downstream process in the value chain. One of the benefits is the considerable improvement in the autoclave by rerouting appropriately different materials, even at a higher transportation cost, the generated better blending and higher recovery at the facility.

Stone et al. (2007) show the intricacies of the Blasor optimizer implemented for the Yandi iron ore mining complex. The optimizations work in steps: aggregation of blocks, extraction sequence and ultimate pit limit definition, mine phase design, and the valuation of the optimal panel extraction sequence. The framework is formulated as mix-integer programming, and the optimizer utilizes a commercial mix-integer programming solver to maximize discounted cash flows while ensuring that production targets are met concerning quantity and quality. Another version of this optimizer is the one described by Zuckerberg et al. (2007), where the extension named BlasorIPD incorporates in-pit waste dumping into the optimization. Under the step-wise optimization approach, during the scheduling phase, the framework adds a new decision to the model regarding the waste movement, where it can go either to an external waste dump or back to the pit in proper locations without sterilizing the ore. The model also considers water table constraints, in such a way that blocks falling below the water table level can only be extracted if this region is refilled before the end of the mine life. Blasor is also applied at an underground coal mining complex (Rocchi et al. 2011). Eight different domains are defined, and each one is inputted as a virtual open pit. The framework evaluates different scenarios designs for feasible underground development and transportation strategies. The application optimizes the coal production and hoisting while considers blend constraints which outperforms the solution of a commercial software.

Zuckerberg et al. (2011) present an application of the LOM planning software Bodor developed for BHP Billiton's Boddington Bauxite mine. The software optimizes the LOM production plan, meeting blending requirements and minimizing the haulage costs while considers capital and operational costs. Due to the characteristics of the deposit, the goal is to define the sequence of extraction of different pods, which can be seen as clusters of bauxite ore that are spread over a large area. An essential aspect of the application is related to the complex environmental constraints which only allow the exploitation of the resource during a specific time of the year due to wind seasonality. Additionally, before mining a specific pod it is necessary to ensure that the crusher is built or redeployed, the conveyor leading the material to the refinery is installed and that the truck fleet size is defined. The optimization reduces the net present cost by 5% compared to a commercial software.

Whittle (2007) and Whittle (2010) describe a global optimization (Prober optimizer), which figures as one of the industry's standard tools to sequence the extraction of multiple deposits with complex blending and processing requirements, but in different steps. First the extraction sequence is defined and then the processing stream decisions are optimized. As the complexity of the model starts to increase, more non-linear the formulation becomes, for that reason the optimizer uses heuristic approaches and different initializations to generate good solutions in a reasonable time.

Chanda (2007) formulates a simplified network flow model that delivers materials from a group of mines to feed metallurgical plants. Several mines, concentrators, smelters, refineries and mineral market are modelled as nodes, and the arcs represent the circuit associated with transportation the material from one node to another. As a result, the optimizer defines the optimal production and routing plan for mine complex, although it does not provide a mine production schedule. A linear network flow model is also applied in Topal and Ramazan (2012) to efficiently optimize the production schedule of a mining district in Australia with more than 100 pits and 13 plants over 50 years. The material from the mines can flow through stockpiles and a set of different processing facilities in the mine complex. The model simplifies non-linear interactions of the network that occurs at processors and stockpiles by making use of grade bins at each location. The optimized model shows a net present value increased by 10 to 20% compared to existing software.

Groeneveld et al. (2010) propose a flexible mixed-integer programming framework to optimize the life-of-the-mine production plan in a mining complex. The application considers an operation with three open-pits, two processing facilities, rail systems, stockpiles and waste dumps, in addition to the options of using two ports with related rail requirements. Considering flexibility related to these options; results show an 85% increase in NPV compared to a mine design that does not consider this flexibility. Additionally, the authors address the incorporation of stochastic parameters such as price, recovery, capital and operating costs, mine equipment, plant and port utilization, but these uncertain parameters are not fully incorporated in the model. The approach optimizes the model independently for each uncertain input, and multiple optimized models provide a sensitivity analysis of possible designs; however, there is not a single optimized model that is risk-resilient or aware under all uncertain scenarios. Additional limitations of the method relate to not considering a multi-element context, or geological uncertainty.

Dagdelen and Traore (2014) consider the transition from open-pit to underground mining in a context of a mining complex operation with six operating open pits, one underground mine, four stockpiles, waste dumps and one processing facility. The approach consists of generating a series of ultimate pits from the existing ones; then a crown pillar is fixed below and remain untouched for protection. The rates of both open pits and underground mine are defined, and the LOM production schedule for both are evaluated. This step is repeated for increasing depths of the open pit envelopes until the NPV of the operation stops increasing.

These industry efforts mentioned above highlight the importance of connecting and controlling multiple components of the mineral value chain and acknowledge the opportunity to improve results with a single simultaneous optimization framework. However, to provide a flexible modelling of the mining complex optimization, these methods make some strong assumptions, from which it is worth mentioning the most important ones: a) the aggregation of blocks to reduce the size of the optimization, b) the use of commercial MIP solvers and c) the use of deterministic inputs. Aggregation is problematic because it homogenizes the spatial distribution of metal within an aggregate; consequently, the meaning of the selectivity scale is lost, which misleads the optimizer to extract equal proportions of the blocks within an aggregate. The second limits the amount of size of the model that the optimizer can handle, restricting the number of binary variables, such as the period of extraction, the integration of uncertainty in grades and limit the modelling of non-linear interactions. Additionally, some methods do not consider the

processing stream optimization together with the sequence of extraction, which prevents the model to fully profit from all the existing synergies in the mining complex. Last but not least, assuming a determinist input of the grade distribution in the deposit prevents the framework from accounting for the geologic risk and variability, which is credited as the primary cause of not meeting production targets and forecasts (Ravenscroft 1992; Dowd 1994, 1997; Vallée 2000; Dimitrakopoulos et al. 2002a; Godoy 2003; Dimitrakopoulos 2011).

Menabde et al. (2007) presents one of the industry's attempt to incorporating uncertainty and variability in a mixed integer programming approach optimizing the LOM production plan in Blasor optimizer. The orebody model is represented as a set of simulated scenarios and used as input in the optimization. The proposed method maximizes the discounted cash flow of the operation by optimizing mine schedule and cut-off. The range of grades is divided into bins, such that blocks falling in the same bin are processed together if mined in the same period. This provides a robust cut-off optimization since an optimal policy is used that is resilient to uncertainty in grades. The stochastic optimization is compared to a deterministic analogue, and the result shows an improvement in NPV of 20% showing the power of stochastic solutions. The model has the same limitations presented by the other versions of Blasor, such as the use of a commercial MIP solver and the aggregation of blocks.

1.4.2 Simultaneous stochastic optimization of mining complexes

Over the last two decades, developments have focused in overcome the limitations discussed above by introducing a framework that effectively considers geologic uncertainty (Godoy 2003; Dimitrakopoulos and Ramazan 2004; Leite and Dimitrakopoulos 2007; Albor and Dimitrakopoulos 2009; Dimitrakopoulos 2011; Ramazan and Dimitrakopoulos 2013), through the use of two-stage stochastic integer programming (SIP) models (Birge and Louveaux 1997). More recently, these models have evolved to the current state-of-the-art simultaneous stochastic optimization framework (Montiel and Dimitrakopoulos 2015, 2017, 2018, Goodfellow and Dimitrakopoulos 2016, 2017; Montiel et al. 2016), overcoming significant limitations in the field. The framework connects all components in a mining complex and can model non-linear interactions at each destination. One of the primary concerns of the framework is the representation of the orebody as a set of stochastic simulations quantifying the uncertainty and variability of the deposit. Unlike past works, the traditional approach of considering an economic

value for a block is shifted to the economic value of products. Herein, blocks have simulated attributes, and the range of possible economic values are defined only at the market, considering all the intermediate interactions, blending for example, and diverse costs throughout the value chain. Defining the true optimal destination of a block does not rely only on the grade content of the mineral driving the mining complex. There are many factors that can impact the actual value of the block in addition to the grade content. In fact, blocks are not processed individually, blending occurs everywhere (also function of secondary and deleterious elements) and is the major driver of this economic profit obtained from the products at the end of the value chain. Additional examples are the period of extraction and processing, location of the processing facility, geometallurgical properties, presence of external sources, different costs, and many others non-linear transformations that it may occur. In fact, any modification in a sequence of extraction impacts all of the subsequent activities downstream. Similarly, a different decision in an operation strategy may affect the conditions that generated the extraction sequence. Major improvement of this new framework is the ability to connect scheduling, decision policies, downstream optimization and transportation in a single model, capitalizing on the synergies available with the interaction of different components.

Montiel and Dimitrakopoulos (2013) present one of the earliest efforts in integrating uncertainty in mining complex optimization. The authors propose a framework that optimize the LOM extraction sequence whose the objective is to minimize deviations from production targets. The case study applies the methodology at the Escondida Norte copper mining complex, Chile. Due to the size of the optimization in terms of decision variables and overall complexity, the authors use the simulated annealing metaheuristic approach to generate good quality solutions. Results showed that compared to the financial forecast provided by a deterministic approach, the method shows only 5% improvement in NPV. Main accomplishment of the method is the ability to substantially reduce deviations from ore and waste production targets when compared to the deterministic schedule. The method needs an initial schedule solution, such that the result of the optimization is dependent on this starting point. It requires a study on which mining sequence to feed the optimization process to randomize the starting point and explore better the solution space. The limitation of the method is related to the objective function that does not explicitly maximize cash flows, and instead minimizes deviations from production targets; thus the model does not fully profit from the maximal upside potential.

Montiel and Dimitrakopoulos (2015, 2017, 2018) present a framework that considers mining, processing and transportation schedules altogether and an efficient heuristic to solve the proposed formulation. In this model, the authors directly incorporate the desire to maximize the discounted cash flow of the mining complex, while minimizing the deviations from production targets. The method considers three perturbations strategies that are performed multiple times and sequentially: a) block-based perturbation, b) operating alternative-based perturbation, and c) transportation system perturbation. In the block-based perturbation, the overall profitability of the block considering all scenarios is ranked. The framework lets the optimizer to decide what is the best destination of the block considering uncertainty and all non-linear transformations across the value chain. The blocks preferably attempt to go to this most processing location, but when interacting with the other blocks on the deposit, this not necessarily is the optimal destination. Thus, the optimizer attempts to bring earlier profitable blocks and to postpone waste. Operating alternative-based perturbation relate changing the operating alternatives at some facilities, for example changing from fine to coarse grinding at the mill, which has a direct impact in throughput and recovery. These operating alternatives allow better control of geometallurgical variables and consequently a better performance and a more realistic modelling of the processing facility. Finally, the transportation system perturbations modify the proportions of materials through the available logistic system to deliver the material from one destination to another, using trucks and pipelines for example. The model is applied to a multi-pit copper operation, and the generated schedule considers the change in operating modes to maximize the performance of the operation. The risk analysis shows a much higher adherence to production targets and the NPV assessment shows a 5% increase compared to the deterministic base case. These decisions (operating modes and transportation strategy) reinforce the non-linear intercorrelation between different aspects in a mining complex, as the decision of increasing the throughput at the cost of lower recovery should be evaluated regarding the financial gains and related capacities. In addition to the above-described operations, Montiel et al. (2016) also integrate underground operations and external supply necessary needed at the autoclave processor for blending purposes.

Goodfellow and Dimitrakopoulos (2016, 2017) present a very flexible formulation of a two-stage non-linear SIP for the optimization of mining complexes. The model is defined in three types of decision variables. In addition to the block extraction sequence decision variable, the model

presents a destination policy decision, where the authors apply the k-means ++ clustering algorithm (Arthur and Vassilvitskii 2007) to pre-process material types with similar characteristics. This clustering allows dynamic decisions regarding destination policies during the optimization and can be understood as an extension of the Menabde et al. (2007) cut-off optimization strategy, instead of defining decision variables based on the binning approach, the clusters are defined on the multi-dimensional space. All the blocks falling in the same cluster are send to the same destination in a specific period. The creation of cluster help with the optimization by reducing the number of processing decisions to be made. The block-based destination presented by Montiel and Dimitrakopoulos (2015) requires one decision variable for each block in each period, but a cluster defines the same decision variable for a big set of blocks. The third type of decision variable is related to processing stream decisions, which are proportions sent from one location to another. These variables are scenario dependent and can represent the flexibility of the operation in reclaiming different quantities from the stockpiles in different stochastic scenarios. The framework uses a modified version of simulated annealing to deal with extraction sequence variables, and then the particle swarm algorithm (Kennedy and Eberhart 1995) is used to optimize the post-extraction decision variables. This second solver algorithm is necessary due to the difficulty of simulated annealing to deal with continuous variables. The framework is particularly flexible allowing the non-linear calculation of attributes (blending, grade-recovery function, geo-metallurgical responses) at any step of the mining complex. The case studies show substantial improvement in risk management and an increase in NPV by including geologic uncertainty and optimizing the whole mining complex simultaneously

A natural extension of this framework is to incorporate demand uncertainty into the framework. Farmer (2016) extends the above formulation to incorporate capital expenditure decisions directly in the objective function. The optimizer is responsible for selecting both mining and processing facility capacities, and results show a significant increase in NPV compared to a pre-determined capacity case. The study also considers impacts of the project financing by considering a streaming contract under and assessed under uncertain price scenarios. Saliba and Dimitrakopoulos (2017) directly account for supply and demand uncertainty during the LOM production scheduling optimization of a mining complex. This results in a stable long-term production schedule resilient to both sources of uncertainty, which can capitalize on extra

production when the price is favourable. Zhang and Dimitrakopoulos (2017) incorporate uncertainty in ore supply and commodity market in a dynamic non-linear optimization model. The mine production scheduling and the material flow planning are optimized separately, but iteratively and interacting with each other. The solution of the mine production schedule defines the input of the material flow in the value chain. The material flow optimization sends a message to the previous message encouraging or discouraging the extraction of certain material types, which triggers a new scheduling optimization. This process cycles until the final solution is stable regarding these two optimizations. Kumar and Dimitrakopoulos (2017) expand the simultaneous optimization of mining complex to incorporate geometallurgical interactions of materials under supply uncertainty. Geometallurgical attributes have substantial influence in throughput, recovery and milling costs; thus incorporating these elements allow for more realistic mine design. Results from the optimization minimize deviation from production targets in a more risk-resilient scenario.

Del Castillo and Dimitrakopoulos (2016) propose a stochastic multivariate destination policy for geometallurgical variables based on cooperative game theory. The idea is to capitalize on the interactions obtained by processing a cluster of blocks. The blocks are considered players and their simulated attributes are accounted to create coalitions and be sent together to the optimized destination. The case study applies the methodology at a copper-gold deposit with six material types and six destinations. The method does not optimize the schedule but improves blending requirements and targets only by optimizing the processing stream decisions and could improve even more by optimizing the mine schedule altogether.

Del Castillo (2018) extends the stochastic simultaneous optimization of a mining complex to a dynamic multistage programming model. The multistage part of the method allows branching the solution if scenarios are different enough. This branching allows the assessment of decision making by providing a probabilistic assessment of taking or not an investment action (e.g. buying an additional crusher). Non-anticipative constraints ensure that all decisions taken are the same until the solution is allowed to branch. The method still makes sure the solution is robust under the geologic scenarios, that is it does not overfit to the simulations used. The formulation considers operational alternatives and also can evaluate capital expenditure decisions of significant financial impact, e.g. increasing truck fleet and buying an additional crusher. The case study presents an example where the dynamic model improves the NPV by 10% compared to the

traditional two-stage SIP model. The idea is to account for possible investments and guide the solution and decision making when more information is available, which can be analyzed in a probabilistic decision-tree.

All the references present in this chapter show powerfull tolls with a high level of flexibility to generate more realistic modelling and planning of mining complexes.

1.5 Goal and Objectives

The goal of the research presented in this thesis is to extend the high-order simulation framework to generate realizations directly at block-support scale and to apply the approach in the optimization of the strategic plan of a gold mining complex. To meet this goal, the following objectives are set:

- Review the technical literature related to orebody modelling using simulation techniques based on multiple point and high-order spatial statistics, and on the integration of geologic uncertainty into the simultaneous stochastic optimization of mining complexes.
- Extend the spatial high-order simulation method to generate realizations directly at the block-support scale and assess its performance.
- Test the effects of the high-order direct block simulation in an application of the life-of-mine optimization of a mining complex.
- Summarize the main contributions and conclusions of the thesis and provide suggestions for future research.

1.6 Thesis Outline

This thesis is organized as follows.

Chapter - 1 presents a review of the simulation methods for orebody modelling, evolving from the second-order simulation methods to approaches based on multiple-point and high-order spatial statistics. Additionally, it also briefly reviews the technical literature linking stochastic simulations and the simultaneous optimization of mining complexes.

Chapter - 2 presents an approach extending high-order simulation methods to generate realizations directly at the block-support scale. Practical aspects of the method are presented through an application at a gold deposit.

Chapter - 3 presents the use and assessment of the high-order direct block simulation method, presented in Chapter - 2, on an application of the simultaneous stochastic optimization of a gold mining complex, highlighting the advantages of the simulation method for the life-of-mine production scheduling optimization.

Chapter - 4 summarizes the overall conclusions and provides suggestions for future research.

Chapter - 2

High-order block support spatial simulation and application at a gold deposit

2.1 Introduction

Stochastic simulation methods are used to quantify spatial uncertainty and variability of pertinent attributes of natural phenomena in the geo-sciences and geo-engineering. Initial simulation methods were based on Gaussian assumptions and second-order statistics of corresponding random field models (Journel and Huijbregts 1978; David 1988; Goovaerts 1997). To address limits of Gaussian approaches, multiple point statistics (MPS) based simulation methods have been introduced (Guardiano and Srivastava 1993; Strebelle 2002; Zhang et al. 2006; Arpat and Caers 2007; Remy et al. 2009; Mariethoz et al. 2010; Mariethoz and Caers 2014; Mustapha et al. 2014; Chatterjee et al. 2016; Li et al. 2016; Zhang et al. 2017) to remove distributional assumptions, as well as to enable the reproduction of complex curvilinear and other geologic features by replacing the random field model with a framework built upon the extraction of multiple point patterns from a training image (TI) or geological analogue. The main limitations of MPS methods are that they do not explicitly account for high-order statistics, nor provide consistent mathematical models while they generate TI-driven realizations. Previous studies have shown resulting realizations that comply with the TI used, but do not necessarily reproduce the spatial statistics inferred from the data (Osterholt and Dimitrakopoulos 2007; Goodfellow et al. 2012). As an alternative to the above limitations, a high-order simulation (HOSIM) framework has been proposed as a natural generalization of the second-order based random field paradigm (Dimitrakopoulos et al. 2010; Mustapha and Dimitrakopoulos 2010a; b, 2011, Minniakhmetov and Dimitrakopoulos 2017a; b; Minniakhmetov et al. 2018; Yao et al. 2018). The HOSIM framework does not make any assumptions about the data distribution, and the resulting realizations reproduce the high-order spatial statistics of the data. Similar to the MPS and most Gaussian simulation approaches, HOSIM methods generate realizations at the point support, whereas, in most major areas of applications, simulated realizations need be at the block support scale. Typically, the change of support needed is addressed by generating simulated realizations at a very dense grid of nodes that is then post-processed to generate realizations at the block

support size needed, which is a computationally demanding process, as related configurations may require extremely dense grids that may be in the order of many millions to billions of nodes. Thus, there is a need for computationally efficient methods that simulate directly at the block support scale.

In the context of the conventional second-order geostatistics, direct block support simulation has been proposed. Godoy (2003) presents an approach, termed "direct block simulation," that discretizes each block into several internal nodes, but only stores a single block value in memory for the next group simulation. This mechanism drastically reduces the amount of data stored in memory and saves considerable computational effort. Boucher and Dimitrakopoulos (2009) expand the sequential direct block simulation method to incorporate multiple correlated variables by applying the min/max autocorrelation function (MAF). Emery (2009) uses an explicit change of the support model and directly simulates at block support. Although efficient, these methods carry all the limitations of a Gaussian simulation framework and related spatial connectivity is limited to two-point spatial statistics, thus, remain unable to characterize non-Gaussian variables, complex non-linear geological geometries and the critically important connectivity of extreme values (Journel 2018). Thus, alternatives are needed.

High-order sequential simulation methods use high-order spatial cumulants to describe complex geologic configurations and high-order connecticity. At the same time, simulated realizations remain consistent with respect to the statistics of the available data, while capitalizing on the additional information that TIs can provide. Dimitrakopoulos et al. (2010) describe these high-order spatial cumulants as combinations of moment statistical parameters. Mustapha and Dimitrakopoulos (2010a) propose a high-order simulation algorithm, where the conditional probabilities density functions (cpdf) are approximated by Legendre polynomials and high-order spatial cumulants. A template is defined based on the central node to be simulated and the nearest conditioning data. The replicates of this configuration are obtained from both the data and TI, and are used as input for the calculation of the Legendre coefficients in the cpdf approximation. Advantages of this method lie in the absence of assumption on the distribution of the data and in being a data-driven approach. Minniakhmetov et al. (2018) replace the Legendre polynomial by Legendre-like splines as the basis function for the estimation of conditional probabilities. Results show a more stable approximation of the related cpdf. Improving upon the computational performance, Yao et al. (2018) propose a new approach, where the calculation of

the cpdf is simplified and no explicit calculation of cumulants is required. Although effective, the methods above are performed at point support scale.

This paper presents a new method that generates high-order stochastic simulations directly at the block support scale. The technique considers overlapping grids representing a study area at two support scales, point and block support, where the simulation process is implemented at the latter support. In the sequential simulation pocess followed, only the initial point support data and previously simulated blocks are added to the set of conditioning values, thus drastically reducing the number of elements stored in memory. The block to be simulated and the nearest conditioning data, at the point or block support, define the spatial configuration of the template used. Similarly, the TI is represented in both support scales to provide replicates of related spatial template configuration. The conditional cross-support joint density function estimated at each block is approximated by Legendre-like splines.

The remainder of the paper is organized as follows. First, the proposed model for high-order block support simulation is presented. Subsequently, a case study in a controlled environment assesses the performance of the current approach. Next, the method is applied to an actual gold deposit to demonstrate its practical aspects. Conclusions follow.

2.2 – High-order block support simulation

2.2.1 – Sequential simulation

In the following description, the index V relates to elements at the block support, while P represents point support. Consider a stationary and ergodic non-Gaussian random field (RF) $Z_P\left(u_j\right)$ in R^n, where u_j defines the location of nodes j in the domain $D \subseteq R^n$. Now consider a transformation function that takes the above point support RF to the block support RF. Any upscaling function can be applied, but assume Eq. 13 for simplicity.

$$Z_V\left(v\right) = \frac{1}{\left|V\right|} \int_{u_j \in v} Z_P\left(u_j\right) du_j. \tag{13}$$

Now, $Z_V\left(v_i\right)$ is also a RF, indexed as $v_i \in D \subseteq R^n, i = 1, \ldots, N_V$ where N_V represents the total number of blocks to be simulated within the domain $D \subseteq R^n$. $Z_V\left(v_i\right)$ is the upscaled RF from

$Z_P(u_j)$ considering all nodes u_j that are discretized within the block centred in v_i, where V is the volume.

The outcomes from the above RFs are denoted as $z_j^P = z_P\left(u_j\right)$ and $z_i^V = z_V\left(v_i\right)$, respectively for the point and the block support RF $Z_P\left(u_j\right) = Z_j^P$ and $Z_V\left(v_i\right) = Z_i^V$. Herein, the objective is to simulate a realization of the RF Z_i^V given the set of initial conditioning values at point support are denoted as $d_p = \left\{z_1^P, \ldots, z_{N_P}^P\right\}$, N_P being the total of conditioning point support values. According to the sequential simulation theory in the geostatistical field, the joint probability density function (jpdf) $f_{Z_1^V,\ldots,Z_k^V}$ can be decomposed in the products of their respective univariate distributions (Johnson 1987; Journel and Alabert 1989; Journel 1994; Goovaerts 1997; Dimitrakopoulos and Luo 2004)

$$\begin{aligned} f_{Z_1^V,\ldots,Z_{N_V}^V}\left(z_1^V, z_2^V, \ldots, z_{N_V}^V \middle| d_P\right) &= f_{Z_1^V}\left(z_1^V \middle| d_P\right) f_{Z_2^V,\ldots,Z_{N_V}^V}\left(z_2^V, \ldots, z_{N_V}^V \middle| d_P, z_1^V\right) \\ &= f_{Z_1^V}\left(z_1^V \middle| d_P\right) f_{Z_2^V}\left(z_2^V \middle| d_P, z_1^V\right) \ldots f_{Z_{N_V}^V}\left(z_{N_V}^V \middle| d_P, z_1^V, z_2^V, \ldots, z_{N_V-1}^V\right). \end{aligned} \tag{14}$$

According to the Eq. 14, each block v^k is simulated based on the estimation of the conditional cross-support probability density function $f_{Z_k^V}\left(z_k^V \middle| d_P, z_1^V, z_2^V, \ldots, z_{k-1}^V\right)$, which according to Bayes' rule (Stuart and Ord 1987) is

$$f_{Z_k^V}\left(z_k^V \middle| d_P, z_1^V, z_2^V, \ldots, z_{k-1}^V\right) = \frac{f_{\mathbf{Z}}\left(d_P, z_1^V, z_2^V, \ldots, z_{k-1}^V, z_k^V\right)}{\int_D f_{\mathbf{Z}}\left(d_P, z_1^V, z_2^V, \ldots, z_{k-1}^V, z_k^V\right) dv_k}. \tag{15}$$

where $\mathbf{Z} = z_1^P, \ldots, z_{N_P}^P, z_1^V, \ldots, z_k^V$. It is sufficient to approximate only the cross-support joint probability density function $f_{\mathbf{Z}}\left(d_P, z_1^V, z_2^V, \ldots, z_{k-1}^V, z_k^V\right)$. In this paper, this cross-support joint probability density function is approximated using Legendre-like orthogonal splines (Wei et al. 2013; Minniakhmetov et al. 2018).

2.2.2 – Joint probability density function approximation

For simplicity, let $f(z)$ be the pdf of a random variable Z defined in $\Omega = [a,b]$ and let $\varphi_1(z), \varphi_2(z), \ldots$ be a set of set of orthogonal functions defined in the same space Ω. Then, a fixed number ω of those orthogonal functions can approximate $f(z)$ (Lebedev 1965; Mustapha and Dimitrakopoulos 2010a; Minniakhmetov et al. 2018) Yao et al. 2018), when multiplied by coefficients L_i.

$$f(z) \approx \sum_{i=0}^{\omega} L_i \varphi_i(z). \tag{16}$$

Since the sets of functions are orthogonal,

$$\int_a^b \varphi_i(z)\varphi_j(z)dz = \delta_{ij}, \tag{17}$$

where δ_{ij} is the Kronecker delta indexed by i and j, such that it gets a unitary value if $i = j$; and 0 otherwise. By using a definition of the expected value of one of a basis function

$$E[\varphi_i(z)] = \int_a^b \varphi_i(z) f(z)dz. \tag{18}$$

Replacing $f(z)$ as in Eq. 16, it is obtained

$$\begin{aligned} E[\varphi_i(z)] \approx \int_a^b \varphi_i(z) \sum_{j=0}^{\omega} L_j \varphi_j(z)dz = \sum_{j=0}^{\omega} L_j \int_a^b \varphi_j(z)\varphi_i(z)dz = \\ = \sum_{j=0}^{\omega} L_j \delta_{ij} = L_i. \end{aligned} \tag{19}$$

L_i coefficient can be experimentally obtained from an available sample, thus $f(z)$ is approximated by Eq.16.

Moving to the multivariate cross-support case, at every block location v^k the cross-support jpdf $f_{\mathbf{Z}}\left(d_P, z_1^V, z_2^V, \ldots, z_{k-1}^V, z_k^V\right)$ can be defined in a similar sense. Considering in practice not all the samples are included as conditioning n_V and n_P are the maximum number of elements at block support and point support, respectively, in the calculation. Moving forward, the above cross-support jpdf is referred as $f\left(z_0^V, \ldots, z_{n_V}^V, z_1^P, \ldots, z_{n_P}^P\right)$ for simplistic notation ensuring a better understanding of variables in both block and point support layers. Also note that, without loss of generality, z_0^V is the value to be simulated at the v_0 location. The cross-support jpdf is defined in the domain $[a,b]^{n_V+1} \times [a,b]^{n_P}$. Note that the interval for the block support is not necessarily the same as the point support. It also applies to the basis functions $\varphi_j(z)$, that could be discretized differently for both supports .Similarly to the univariate case, the cross-support jpdf can be approximated as

$$f\left(z_0^V, \ldots, z_{n_V}^V, z_1^P, \ldots, z_{n_P}^P\right) \approx$$
$$\sum_{k_0^V}^{\omega} \cdots \sum_{k_V^{n_V}}^{\omega} \sum_{k_P^1}^{\omega} \cdots \sum_{k_P^{n_P}}^{\omega} \left[L_{k_0^V \ldots k_{n_V}^V k_1^P \ldots k_{n_P}^P} \varphi_{k_0^V}\left(z_0^V\right) \ldots \varphi_{k_{n_V}^V}\left(z_{n_V}^V\right) \varphi_{k_1^P}\left(z_1^P\right) \ldots \varphi_{k_{n_P}^P}\left(z_{n_P}^P\right) \right]. \quad (20)$$

Those $L_{i \ldots jk \ldots l}$ coefficients can be calculated experimentally since they can be obtained from the orthogonality property of the basis functions. Following the definition of the expected value of a basis function, it is expressed as:

$$E\left[\varphi_i\left(z_0^V\right) \ldots \varphi_j\left(z_{n_V}^V\right) \varphi_k\left(z_1^P\right) \ldots \varphi_l\left(z_{n_P}^P\right)\right] =$$
$$\int_a^b \cdots \int_a^b \int_a^b \cdots \int_a^b \varphi_i\left(z_0^V\right) \ldots \varphi_j\left(z_{n_V}^V\right) \varphi_k\left(z_1^P\right) \ldots \quad (21)$$
$$\varphi_l\left(z_{n_P}^P\right) f\left(z_0^V, \ldots, z_{n_V}^V, z_1^P, \ldots, z_{n_P}^P\right) dz_0^V \ldots dz_{n_V}^V dz_1^P \ldots dz_{n_P}^P.$$

Replacing $f\left(z_V^0, \ldots, z_V^{n_V}, z_P^1, \ldots, z_P^{n_P}\right)$ as in Eq. 20, it is obtained

$$E\left[\varphi_i\left(z_0^V\right)\ldots\varphi_j\left(z_{n_V}^V\right)\varphi_k\left(z_1^P\right)\ldots\varphi_l\left(z_{n_P}^P\right)\right]\approx$$

$$\int_a^b\ldots\int_a^b\int_a^b\ldots\int_a^b\varphi_i\left(z_0^V\right)\ldots\varphi_j\left(z_{n_V}^V\right)\varphi_k\left(z_1^P\right)\ldots\varphi_l\left(z_{n_P}^P\right)\sum_{k_0^V}^{\omega}\ldots\sum_{k_{n_V}^V}^{\omega}\sum_{k_1^P}^{\omega}\ldots$$

$$\sum_{k_{n_P}^P}^{\omega}\left[L_{k_0^V\ldots k_{n_V}^V k_1^P\ldots k_{n_P}^P}\varphi_{k_0^V}\left(z_0^V\right)\ldots\varphi_{k_{n_V}^V}\left(z_{n_V}^V\right)\varphi_{k_1^P}\left(z_1^P\right)\ldots\varphi_{k_{n_P}^P}\left(z_{n_P}^P\right)\right]dz_0^V\ldots dz_{n_V}^V dz_1^P\ldots dz_{n_P}^P=$$

$$\sum_{k_0^V}^{\omega}\ldots\sum_{k_{n_V}^V}^{\omega}\sum_{k_1^P}^{\omega}\ldots\sum_{k_{n_P}^P}^{\omega}\left[L_{k_0^V\ldots k_{n_V}^V k_1^P\ldots k_{n_P}^P}\int_a^b\ldots\int_a^b\int_a^b\ldots\int_a^b\varphi_i\left(z_0^V\right)\varphi_{k_0^V}\left(z_0^V\right)\ldots\right. \tag{22}$$

$$\left.\varphi_j\left(z_{n_V}^V\right)\varphi_{k_{n_V}^V}\left(z_{n_V}^V\right)\varphi_k\left(z_1^P\right)\varphi_{k_1^P}\left(z_1^P\right)\ldots\varphi_l\left(z_{n_P}^P\right)\varphi_{k_{n_P}^P}\left(z_{n_P}^P\right)\right]dz_0^V\ldots dz_{n_V}^V dz_1^P\ldots dz_{n_P}^P=$$

$$\sum_{k_0^V}^{\omega}\ldots\sum_{k_{n_V}^V}^{\omega}\sum_{k_1^P}^{\omega}\ldots\sum_{k_{n_P}^P}^{\omega}\left[L_{k_0^V\ldots k_{n_V}^V k_1^P\ldots k_{n_P}^P}\delta_{ik_0^V}\ldots\delta_{jk_{n_V}^V}\delta_{k k_1^P}\delta_{l k_{n_P}^P}\right]=L_{i\ldots jk\ldots l}.$$

Now, to determine $L_{i\ldots jk\ldots l}$, the expected value from Eq. 22 is calculated from replicates of the training image according to a template defined from simulation grid and sampling data.

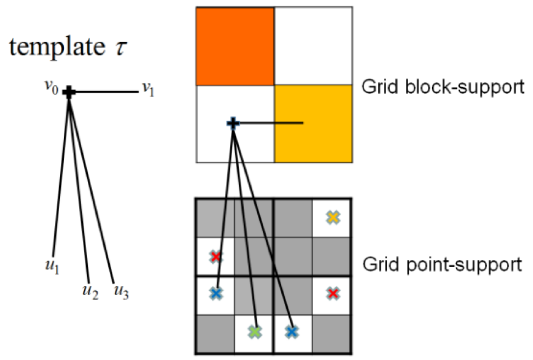

Figure 2.1 – An example of a template τ with conditioning data capturing values in both point and block support sizes.

Let $\tau=\left[v_0,\ldots,v_{n_V},u_1,\ldots,u_{n_P}\right]$ be a template as in Fig. 2.1, where v_0 and v_1 represent locations at block support, and u_1,u_2 and u_3 represent point support locations. v_0 is the location of the block to be simulated and n_P and n_V are, respectively, the total number of points and blocks

used as conditioning. In the figure the grids at point and block support appear separated, but this is only for visualization purporses. In reality, they overlap each other and the distance between layers is set to 0. τ is defined considering limited conditioning values, which are chosen in order of Euclidean proximity from the central block to be simulated. Having the specified template τ, the TI is scanned, and the replicates of such template are retrieved. Note that τ has elements that belong to the point and block support sizes. Similarly, the TI requires to be available both scales. Therefore, assuming a TI input in the point support scale, it is rescaled to block support, and both are retrieved during the simulation process, each one in its respective layer.

The algorithm for the block support high-order simulation method is as follows:

1. Upscale the TI from point to block support.
2. Define a random path to visit all the unsampled block locations on the simulation grid.
3. At each v^0 block location:
    a. Find the nearest conditioning point and block support values.
    b. Obtain the template τ according to the configuration of the central block and related conditioning values in both support sizes.
    c. Scan the training images, searching for replicates of the template τ and corresponding values.
    d. Calculate all the spatial cross-support coefficients $L_{i\ldots jk\ldots l}$ using Eq. 22.
    e. Derive the conditional cross-support jpdf $f_{Z_0^V}\left(z_0^V \middle| d_P, z_1^V, z_2^V, \ldots, z_k^V\right)$ according to Eqs. 20 and 15.
    f. Draw a uniform value from $\left[0,1\right]$ to sample z_0^V from the conditional cumulative distribution derived from the above.
    g. Add z_0^V to the simulation grid at block support scale so that it can be a conditioning value for the next block.
4. Repeat steps 2 and 3 for additional realizations.

2.2.3 Approximation of a joint probability density using Legendre-like orthogonal splines

The current paper uses the Legendre-like splines (Wei et al. 2013; Minniakhmetov et al. 2018) as means to obtain the basis function above mentioned. In short, those splines are a combination of Legendre polynomials (Lebedev 1965) up to the r^{th} order and linear combinations of B-splines(de Boor 1978). B-splines are a particular class of piecewise polynomials (splines) connected by some condition of continuity, and by itself do not form an orthogonal basis. Thus, as introduced in Wei et al. (2013), the first $r+1$ splines are the Legendre polynomials, which can be defined as in (Lebedev 1965)

$$\varphi_r = \frac{1}{2^r r!}\left(\frac{d^r}{dz^r}\right)\left[\left(z^2-1\right)^r\right], \quad -1 \le z \le 1. \tag{23}$$

The additional functions are constructed given the domain T

$$T = \{\underbrace{a,a,\ldots,t_0=a}_{r+1} < t_1 \le t_2 \le \ldots \le t_{m_{\max}} < \underbrace{t_{m_{\max}+1}=b,b,\ldots,b}_{r+1}\}, \tag{24}$$

where the t_i elements are referred to as knots and $m_{\max}$ represents the maximum number of knots. The final Legendre-like splines are defined as

$$\varphi_{r+m}(t) = \frac{d^{r+1}}{dt^{r+1}} f_m(t), \quad m = 1 \ldots m_{\max}, \tag{25}$$

The $f_m(t)$ is the determinant of the following matrix

$$f_m(t) = \det\begin{pmatrix} B_{-r,2r+1,m}(t) & B_{-r+1,2r+1,m}(t) & \cdots & B_{-r+m-1,2r+1,m}(t) \\ B_{-r,2r+1,m}(t_1) & B_{-r+1,2r+1,m}(t_1) & \vdots & B_{-r+m-1,2r+1,m}(t_1) \\ \vdots & \vdots & \ddots & \vdots \\ B_{-r,2r+1,m}(t_{m-1}) & B_{-r+1,2r+1,m}(t_{m-1}) & \cdots & B_{-r+m-1,2r+1,m}(t_{m-1}) \end{pmatrix}, \tag{26}$$

which is constructed with the auxiliary splines $B_{i,r,m}(t)$, of r^{th} order, obtained according to the recursive rule

$$B_{i,0,m} = \begin{cases} 1, & t_{i,m} \le t \le t_{i+1,m} \\ 0, & \text{otherwise} \end{cases},$$
$$B_{i,r,m}(t) = \frac{t - t_{i,m}}{t_{i+r-1,m} - t_{i,m}} B_{i,r-1,m}(t) + \frac{t_{i+r,m} - t}{t_{i+r,m} - t_{i+1,m}} B_{i+1,r-1,m}(t). \quad (27)$$

These auxiliary functions are defined on the knot sequence $T_m = \{t_{i,m}\}_{i=-r}^{r+m+1}$, $m = 1 \ldots m_{\max} - 1$ and the $t_{i,m}$ term is defined as

$$t_{i,m} = \begin{cases} a, & -r \le i \le 0 \\ t_i, & 1 \le i \le m \\ b, & m+1 \le i \le m+r+1 \end{cases}. \quad (28)$$

2.3 – Testing with an exhaustive dataset

The method outlined above is tested using the two-dimensional image of the Walker-Lake dataset (Isaaks and Srivastava 1989). The exhaustive dataset comprises two correlated variables *U* and *V* of sizes 260x300 pixels. Random stratified sampling is used to retrieve 234 values from or 0.3% of the exhaustive image *V* to be used as the data set in the direct block simulation of *V*, to test the proposed method. The full dataset *V* is converted from the point to a block support representation by an averaging over 5x5 pixels. This block support version is referenced here as the fully-known reference image and it is used for comparisons. Figure 2.2 shows *V* at the point and block support scale, as well as the dataset to be used. The image *U* is chosen as the training image in the simulation process. Figure 2.3 presents the TI in both point and block support (5x5 unit size) scales. To help the method find more meaningful spatial patterns of the potential conditioning templates, the histogram of TI is matched to the dataset one. Histograms of the exhaustively known image, TI and dataset are displayed in Fig. 2.4 and basic statistics are presented in Table 2.1.

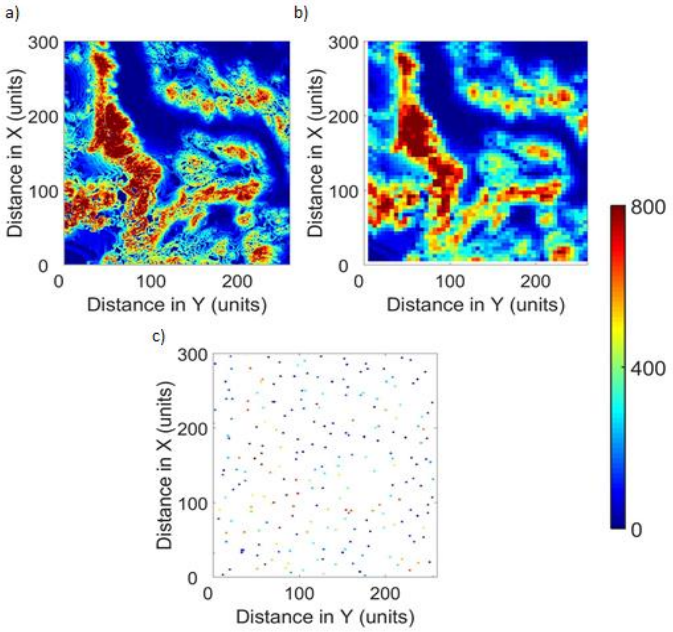

Figure 2.2 - Exhaustive image "*V*" (a) at point support, (b) at block support, and (c) 234 samples from image in (a) – 234 samples

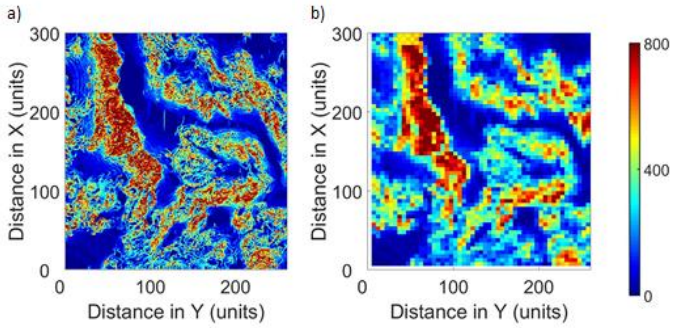

Figure 2.3 – Training image "*U*" at the (a) point support scale, and (b) block support scale.

Table 2.1 – Basic stats of dataset, training image and fully known image at point support scale.

Basic stats	Dataset	Reference image	Training image
Average	277.0	278	278.5
Median	193.5	221.3	193.6
Variance	68926	62423	70385

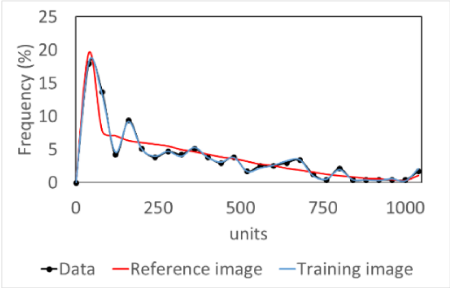

Figure 2.4 – Histogram of data, reference and training image at point support scale.

The test conducted consists of generating 15 simulated realizations of the *V* dataset at block support, using the data and the training image mentioned above. Figure 2.5 presents three of the simulated realizations generated and Table 2 shows the statistics relative to the average of the 15 simulations, training image and reference image at block scale. A comparison of Figs. 2(b) and 5 suggest that the simulations reproduce the main structures of low and high values of the fully-known reference image *V*. The histograms and variograms presented in Figs. 2.6 and 2.7 respectively reasonably follow the behaviour exhibited by the variogram model from the data and the training image. Note that the variograms of data is computed at point scale and rescaled to represent the corresponding volume-variance relation (Journel and Huijbregts 1978).

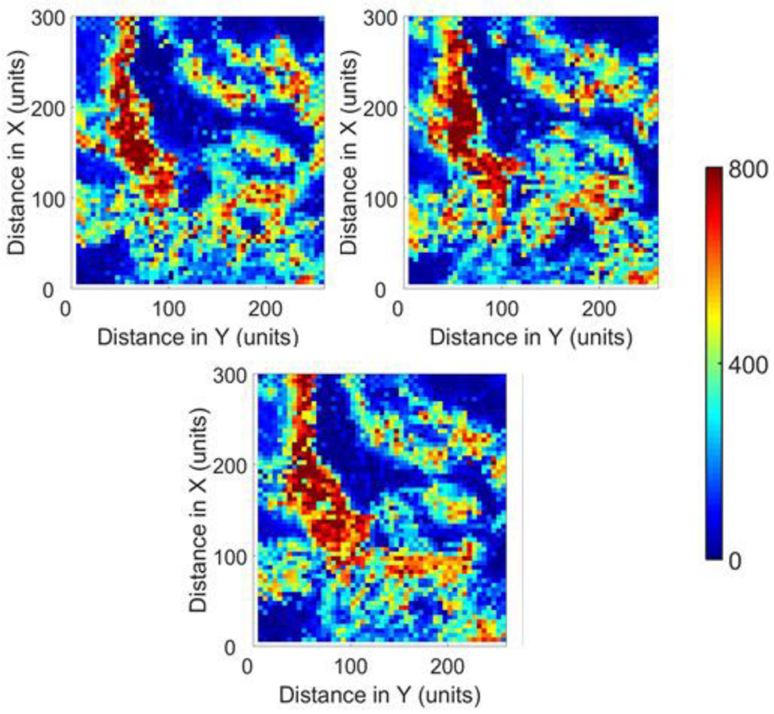

Figure 2.5 – Example of 3 simulated realizations of the Walker Lake reference image *V*.

Table 2.2 - Basic stats of the average of the simulations, training image and reference image at block support scale

Basic stats	Simulations	Training image	Reference image
Average	280.6	278.5	278.0
Median	234.6	237.0	235.4
Variance	51764	46518	52304

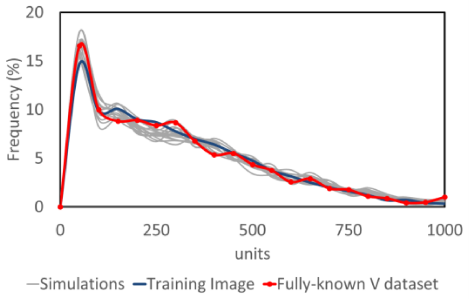

Figure 2.6 –Histograms of the simulations at block support, and comparison with reference and training image also at block support.

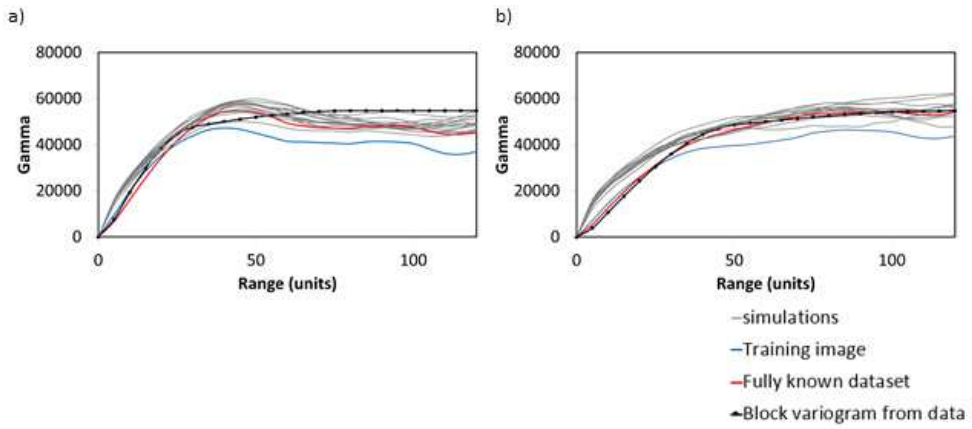

Figure 2.7 – Variograms of simulated realizations, exhaustive image, TI, and variogram from data rescaled to block support variance; figure (a) shows the WE direction, and (b) the NS direction.

Spatial cumulants (Dimitrakopoulos et al. 2010) quantify the spatial relationships between three and more points and are used herein to assess high-order spatial patterns. The third-order cumulant maps are presented along with the template used for its calculation in Fig. 2.8. Figure 2.9 shows the fourth-order cumulant map, where three slices of the complete cumulant map and the related template are displayed. In both figures, the colors range from blue to red, representing lower to higher spatial inter-correlation between values. Note that the reference and training image high-order maps are calculated on the block support scale, while the cumulant maps related to each simulation is averaged to a single map using the 15 stochastic simulated realizations at block support. During the calculation of the high-order spatial statistics from the data, only a few replicates are obtained and Fig. 2.8a presents a smooth interpolation using B-splines. Regarding the third-order maps, the average of the simulations match the spatial features observed in the data and fully-known dataset. It also shares similarities with the third-order cumulants map from TI, this is somewhat expected as the process captures high-order relations from the TI at block support at well. These spatial relations present in the TI ended up being present in the realizations as well.

The fourth-order cumulant map reproduces the characteristics that are closer to the TI than the fully-known image, as expected. Note that, by explicitly calculating the spatial high-order cumulants, the information received from the training image to infer local cross-support distributions is conditioned to the data.

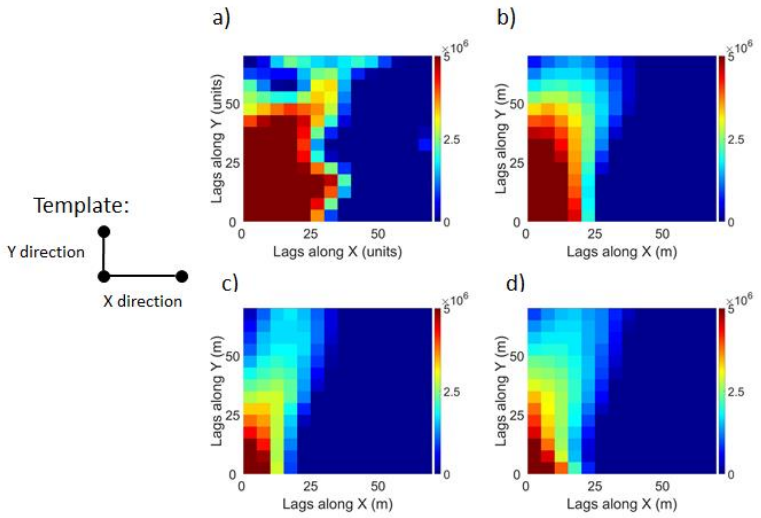

Figure 2.8 - Third-order cumulant maps for (a) point support data used, (b) fully-known block support image *V*, (c) training image, and (d) the average map of the 15 simulated realizations.

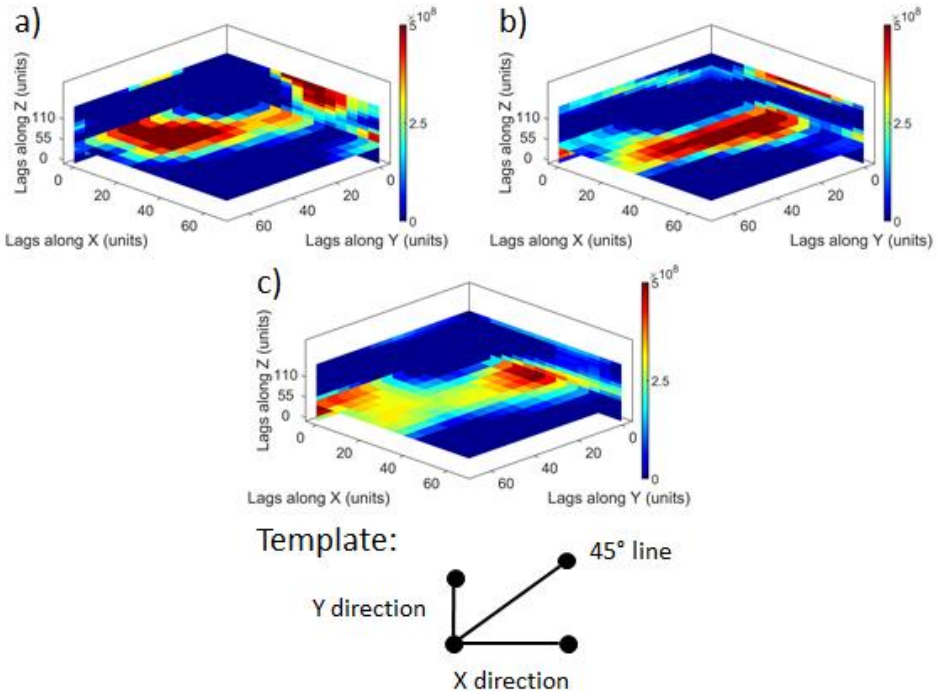

Figure 2.9 - Slices of the fourth-order cumulant maps for (a) fully-known image *V*, (b) training image, and (c) average map of the 15 simulations, all at block support.

2.4 – Applications at a gold deposits

This section applies the proposed method at a gold deposit. The dataset comprises 2,300 drillholes that are spaced approximately at a 35 x 35 m^2 configuration covering an area of 4.5 km^2. The training image is defined on $405 \times 445 \times 43$ grid blocks of size $5 \times 5 \times 10$ m^3 and is based on blasthole samples. Both inputs are composited in a 10 m bench and are considered to be at point support. Figure 2.10 presents the drillholes available and the training image at block scale. The deposit to be simulated is represented by 510,800 blocks measuring 10x10x10 m^3 each.

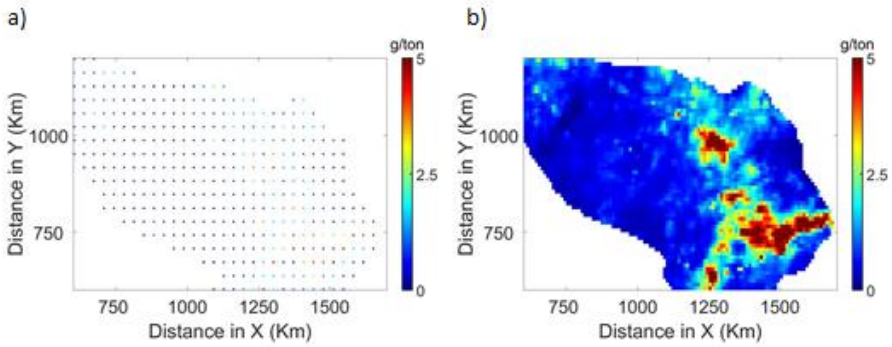

Figure 2.10 – (a) Cross-section of the available drillhole locations, and (b) training image in the block support scale.

Table 2.3 - Basic stats of the average of the simulations and training image at block support and dataset at point scale

Basic stats	Simulations	TI block support	Data point support
Average	0.63	0.62	0.63
Median	0.40	0.39	0.39
Variance	0.74	0.76	1.81

Fifteen simulated realizations are generated and cross-sections from two of them are presented in Fig. 2.11 to show similarities with the data and TI in the corresponding cross-section in Fig. 10. Notable is the reproduction of a sharp transition from high to low grades. Figure 2.12 shows the histograms of the simulations and TI at block support. Table 3 provides the related statistics. Variograms at block support are displayed in Fig. 2.13, where the data variogram is regularized to reflect the corresponding volume-variance relation. The second-order spatial statistics of the

simulations match reasonably with the pattern followed by the data and are close to those of the TI. Results for third- and fourth-order cumulants and related maps for the data, TI and simulated realizations are shown in Figs. 2.14 and 2.15, respectively. It is noted that the high-order statistics of the simulated realizations match those of the data and TI.

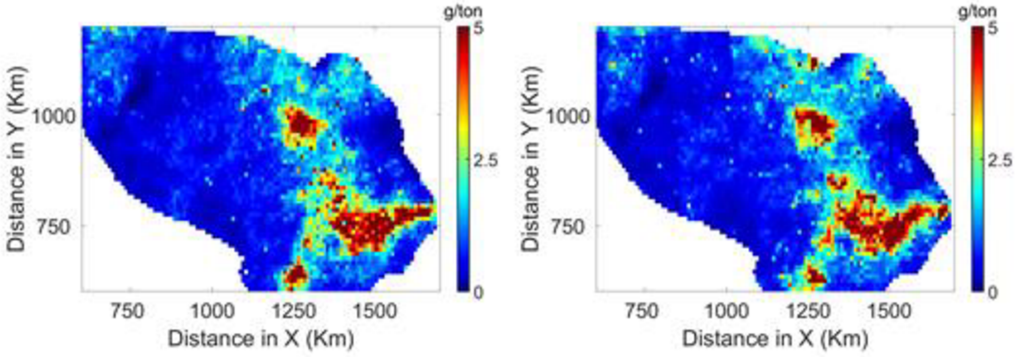

Figure 2.11 - Cross-section of two simulated realizations.

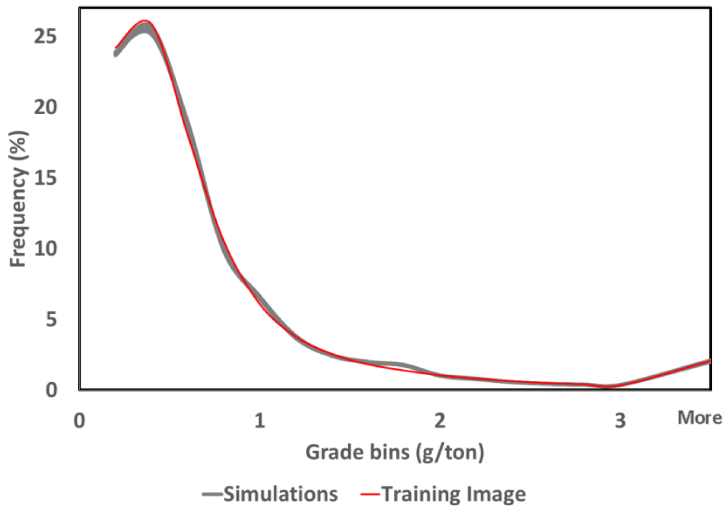

Figure 2.12 - Histograms of simulated realizations and training image.

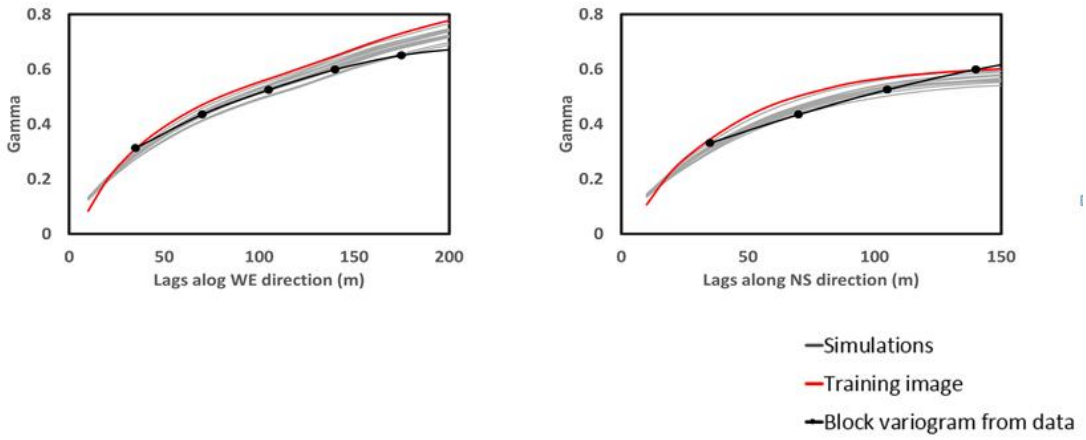

Figure 2.13 - Variograms of simulated realizations and training image and data variograms rescaled to represent block variance; WE direction (left) and NS direction (right).

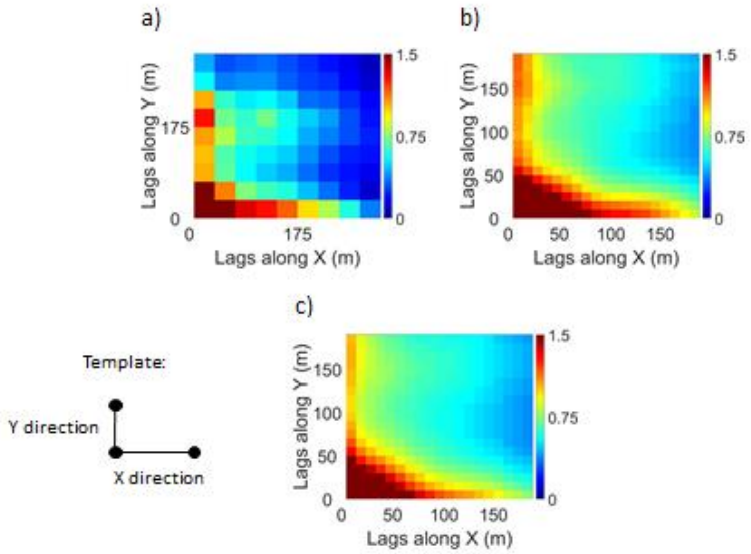

Figure 2.14 - Third-order cumulant maps, obtained with the template in the left, for the (a) dataset, (b) training image at block support, and (d) average map of the 15 simulations.

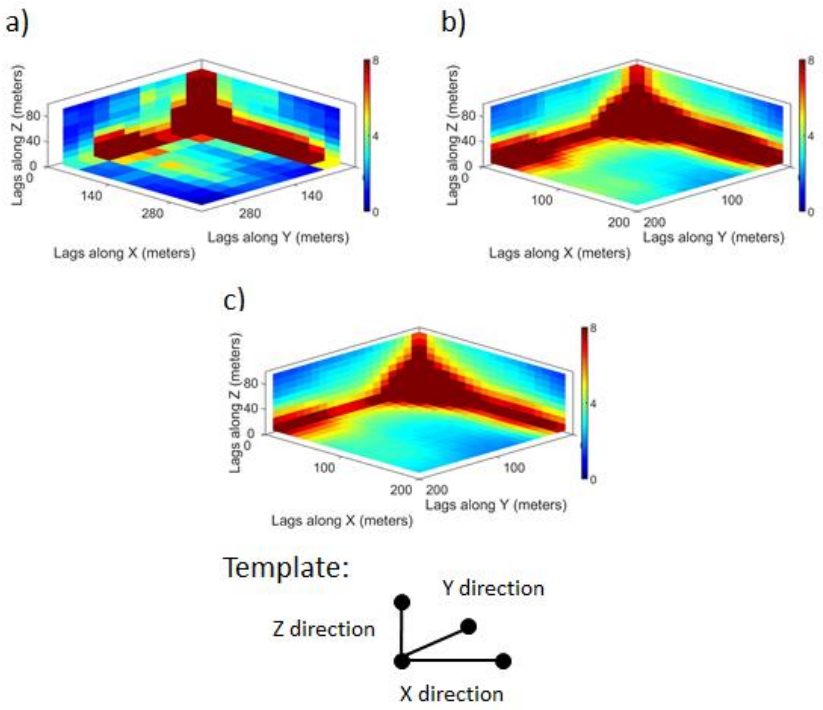

Figure 2.15 - 3 slices of the fourth-order cumulant maps, obtained with the template in the bottom, for the (a) dataset, (b) training image at block support, and c) average map of the 15 simulations.

Further highlighting the advantages of the proposed direct block high-order simulation method, one may note that, for the above case study, the run time of the related algorithm was approximately five and a half hours, while the point high-order simulation requires approximately twenty-four hours. Both approaches are tested with the same specifications and computing equipment: Intel® Core™ i7-7700 CPU with 3.60 GHz, 16GB of RAM and running under Windows 7.

2.5 – Conclusions

This paper presented a new high-order simulation method that simulates directly at block support scale by estimating, at every block location, the cross-support joint probability density function. Legendre-like splines are the set of a basis function used to approximate the above density function. The related coefficients are calculated from replicates of a spatial template employed. The latter template is generated from the configuration of the block to be simulated and associated conditioning values, whose supports can be both at the point and block support scales.

The high-order character of the proposed direct block simulation method ensures that generated realizations reflect complex, non-linear spatial characteristics of the variables being simulated and reproduce the connectivity of extreme values.

The proposed algorithm was tested using an exhaustive image showing that the different realizations generated can reasonably reproduce spatial architectures observed in the exhaustive image. An application at a gold deposit shows the practical aspects of the method. In addition, it documents that the method works well while simulated realizations are shown to reproduce the spatial statistics of the available data up to the cumulants of the fourth-order that were calculated. Further work will focus on improving computational efficiency, generating training-images that are consistent with the high order relations in the available data, and extending the proposed method to jointly simulate multiple variables.

Chapter - 3

Effects of high-order simulations on the simultaneous stochastic optimization of mining complexes

3.1 Introduction

A mining complex can be perceived as a transfer function that encapsulates complex interactions starting from the extraction of material from the mines until its transformation in sellable products, passing through different processes in the mineral value chain (Montiel and Dimitrakopoulos 2015; Goodfellow and Dimitrakopoulos 2017). It can include, for example, multiple mines, various elements and material types, stockpiles, tailings facilities, waste dumps, processing plants and transportation systems (Pimentel et al. 2010). Simultaneous stochastic optimization of a mining complex maximizes the global value of the mining operation by integrating all the components in a single framework, while including supply uncertainty and variability of materials from the mines as a set of stochastically generated realizations (Montiel and Dimitrakopoulos 2013, 2015, Goodfellow and Dimitrakopoulos 2016, 2017; Montiel et al. 2016; Del Castillo 2018).

Efforts in the industry modelling large mining operations as an integrated mathematical model have been leveraged over the last three decades. Newmont Mining Corporation becomes the pioneer proposing a linear programming approach to the massive mining complex at Nevada (Hoerger et al. 1999). BHP also provide significant improvements with the Blasor optimizer, a BHP Billiton's in-house software applied to Yandi mine complex (Stone et al. 2007) optimizing the life-of-mine sequence of extraction of multiple pits altogether. Additional applications have extended the software to optimize and assess more complex requirements, for example, in-pit dumping (Zuckerberg et al. 2007) and underground mines (Rocchi et al. 2011). Whittle (2007) and Whittle (2010) describe one of the industry standard tools to sequence the extraction of material from multiple deposits in operations with complex blending and processing requirements. Although the methods mentioned above represent significant efforts in integrating multiple components of the mining complex, they still present simplifications and shortcuts. Some frameworks still consider a step-wise optimization of some components leading to suboptimal solutions (Whittle 2007, 2010; Pimentel et al. 2010; Goodfellow and

Dimitrakopoulos 2017). Another limitation is the aggregation of mining blocks, with the purpose to alleviate the optimization part, which can misrepresent the mining selectivity. Additionally, the uncertainty in material supply coming from the mines has been credited as the primary cause of risk in mining operations, and not directly accounting for it during the optimization can lead to unexpected deviations in production targets (Ravenscroft 1992; Dowd 1994; Dimitrakopoulos et al. 2002b; Dimitrakopoulos 2011).

The spatial uncertainty and variability of attributes in geosciences can be quantified via geostatistical simulations (Journel and Huijbregts 1978; David 1988; Goovaerts 1997; Mariethoz and Caers 2014; Rossi and Deutsch 2014), which are founded on the concept of random fields. The sequential simulation approach is an alternative to assess these attributes at each unsampled location of a three-dimensional block model, through Monte Carlo sampling from a conditional distribution function (Journel and Huijbregts 1978; David 1988; Goovaerts 1997). Traditional simulation methods are based on the second-order statistics, namely, mean and covariance (variogram), where sequential Gaussian simulation (SGS) (Isaaks 1990; Journel 1994; Goovaerts 1997), sequential indicator simulation (SIS) (Alabert 1987; Goovaerts 1997) and sequential direct block simulation (Godoy 2003; Boucher and Dimitrakopoulos 2009) are some examples. However, geological attributes of spatially distributed phenomena are represented by complex, non-Gaussian and non-linear spatial connectivity of low and high-grades. Only two statistical parameters (second-order) are not sufficient to fully describe these attributes (Journel 2007). Also, simulation methods that work in the Gaussian space maximize the spatial disorder (maximal entropy) of the realizations, (Journel and Deutsch 1993) preventing a more realistic quantification of the connectivity of high-grades.

Attempting to address these limitations multiple-point statistics (MPS) based simulation methods have been introduced (Guardiano and Srivastava 1993; Strebelle 2002; Journel 2005; Zhang et al. 2006; Arpat and Caers 2007; Remy et al. 2009; Mariethoz et al. 2010; Mariethoz and Caers 2014; Chatterjee et al. 2016). By replacing the random field model with a framework extracting multiple point patterns from a training image (TI), or geological analogue, MPS methods can reproduce complex curvilinear and other geologic features, without making distributional assumptions. However, by mostly extracting patterns from the TI, the approach generates TI-driven realizations, where previous studies have shown that they do not always reproduce the spatial statistics inferred from the data (Osterholt and Dimitrakopoulos 2007; Goodfellow et al.

2012). As a natural extension of second-order methods, the high-order simulation framework (Dimitrakopoulos et al. 2010; Mustapha and Dimitrakopoulos 2010a, 2011, Minniakhmetov and Dimitrakopoulos 2017a; b; de Carvalho et al. 2018; Minniakhmetov et al. 2018; Yao et al. 2018) can reproduce very complex non-linear geometries and spatial statistics from data, by explicitly calculating high-order spatial cumulants. The generated realizations present more realistic and structured connectivity of high grades (lower entropy) compared to traditional methods, as shown in the example in Fig. 3.1.

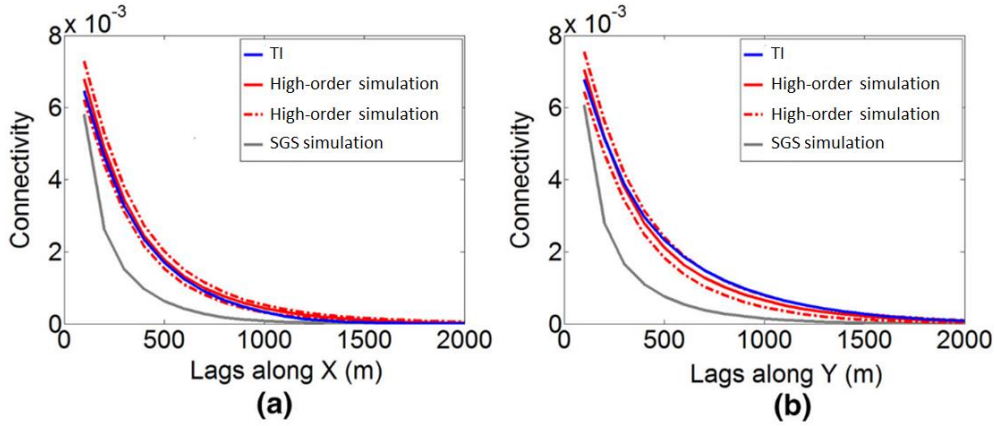

Figure 3.1 – Connectivity of high-grades along X (a) and Y (b) direction, calculated for the 99th percentile. Adapted from Minniakhmetov et al. (2018).

Appropriate characterization of spatial connectivity and its impact in transfer functions are well-studied subjects in flow modelling of reservoirs and aquifers (Journel and Alabert 1989; Journel and Deutsch 1993; Gómez-Hernández and Wen 1998; Renard and Allard 2013). In the mining context, some studies have shown that the use of different simulation frameworks has impacts on the output of transfer functions (Qureshi and Dimitrakopoulos 2005; Dimitrakopoulos and Godoy 2014). Geostatistical simulations have been effectively incorporated into the state-of-the-art simultaneous stochastic optimization of mining complex framework (Montiel and Dimitrakopoulos 2013, 2015, 2017, Goodfellow and Dimitrakopoulos 2016, 2017). The next step is to further investigate the effects of high-order simulation models in this optimization framework.

This paper presents an application of the high-order direct block-support simulation method (de Carvalho et al. 2018) used as input in the simultaneous stochastic optimization of a simplified

mine complex, whose framework is proposed by Goodfellow and Dimitrakopoulos (2016). As a means of comparison, the same mine complex setting is optimized using simulations obtained with a second-order method. First, generated simulations with both methods are compared regarding the spatial connectivity of high grades. Then, differences concerning the life-of-mine production schedule and related production forecasts, optimized for each case, are analyzed and discussed. Next sections provide a brief description of the high-order direct block simulation framework and the optimization model. Subsequently, a comprehensive analysis of the differences presented by both results is presented. Conclusion follows

3.2 Methods

3.2.1 Modelling a mineral deposit using geostatistical simulations

Considering a random function (RF) $Z^p(x_i), x_i \in R^d$, where x_i represents the location of the point support grid to be simulated in the domain $D \in R^d$ and z_i^p a realization of $Z^p(x_i)$. The set of initial data is given by $d_n = \{z^p(x_k), k = 1,\ldots,n\}$ and represents the values obtained from the exploration data. Now consider the set Λ_i with the data and previously simulated nodes, i.e. $\Lambda_0 = \{d_n\}$ and $\Lambda_i = \{\Lambda_{i-1} \cup Z(x_i)\}$. Thus, under the sequential simulation framework (Johnson 1987; Journel and Alabert 1989; Journel 1994; Goovaerts 1997; Dimitrakopoulos and Luo 2004) the global conditional distribution can be decomposed in the multiplication of the univariate distributions:

$$f(x_1,\ldots,x_n; z_1^v,\ldots,z_n^v|\Lambda_0) = f(x_1; z_1^p|\Lambda_0) * \ldots * f(x_n; z_n^p|\Lambda_{n-1}) \quad (29)$$

3.2.1.1 High-order direct block simulation

Instead of simulating the entire deposit at the point support discretization, de Carvalho et al. (2017) present an alternative to generating high-order simulations directly at the scale of blocks. Assume z_i^v a realization of the RF $Z^v(v_i)$ at the block support, defined in the same domain $D \in R^d$, where v_i represents the centroid of the block in consideration. Additionally, the

conditional distribution is derived directly at the block support $f\left(v_i; z_i^v \middle| \Lambda_0, \Lambda_{i-1}^v\right)$, where $\Lambda_{j-1}^v = \left\{z^v\left(v_m\right), m = 1, \ldots, j-1\right\}$ is the set of previously simulated blocks.

The cross-support $f\left(v_i; z_i^v \middle| \Lambda_0, \Lambda_{i-1}^v\right)$ distribution is simplified according to Bayes rule as:

$$f\left(v_i; z_i^v \middle| \Lambda_0, \Lambda_{i-1}^b\right) = \frac{f\left(v_i, \lambda_0, \lambda_{i-1}^b; z_i^v, \Lambda_0, \Lambda_{i-1}^b\right)}{\int f\left(v_i, \lambda_0, \lambda_{i-1}^b; z_i^v, \Lambda_0, \Lambda_{i-1}^b\right) dv_i} \tag{30}$$

where λ_0 and λ_{i-1}^b are the set of locations of Λ_0 and Λ_{i-1}^b, respectively.

For simplicity, $f\left(v_i, \lambda_0, \lambda_{i-1}^b; z_i^v, \Lambda_0, \Lambda_{i-1}^b\right)$ is referred herein as:

$$f\left(v_i, \lambda_0, \lambda_{i-1}^b; z_i^v, \Lambda_0, \Lambda_{i-1}^b\right) = f\left(z_i^v, \underbrace{\left\{z_1^p, \ldots, z_n^p\right\}}_{\text{exploration data}}, \underbrace{\left\{z_1^v, \ldots, z_{i-1}^v\right\}}_{\text{previously simulated blocks}}\right) = f\left(z_1^v, \ldots, z_i^v, z_1^p, \ldots, z_n^p\right) \tag{31}$$

Thus, the above is approximated as:

$$f\left(z_1^v, \ldots, z_i^v, z_1^p, \ldots, z_n^p\right) \approx$$
$$\sum_{k_1^v}^{\omega} \cdots \sum_{k_i^v}^{\omega} \sum_{k_1^p}^{\omega} \cdots \sum_{k_n^p}^{\omega} \left[L_{k_1^v \ldots k_i^v k_1^p \ldots k_n^p} \varphi_{k_0^v}\left(z_1^v\right) \cdots \varphi_{k_{n_i}^v}\left(z_i^v\right) \varphi_{k_1^p}\left(z_1^p\right) \cdots \varphi_{k_n^p}\left(z_n^p\right) \right] \tag{32}$$

where $\varphi_m(\bullet)$ belongs to the set of Legendre-like orthogonal splines (Wei et al. 2013; Minniakhmetov et al. 2018), and the coefficient $L_{i \ldots jk \ldots l}$. is approximated experimentally by:

$$L_{i \ldots jk \ldots l} \approx E\left[\varphi_i\left(z_0^V\right) \cdots \varphi_j\left(z_{n_V}^V\right) \varphi_k\left(z_1^P\right) \cdots \varphi_l\left(z_{n_P}^P\right)\right] \tag{33}$$

The method assumes a TI represented in both support sizes, point and block. Thus, having a spatial template obtained with the block to be simulated and neighbouring values, at the point and block support, this TI is scanned searching for replicates of the template in consideration. The algorithm for the block support high-order simulation can be summarized as:

1. Upscale the TI inputted at point support to the block support.
2. According to the sequential simulation framework, define a random path to visit all the unsampled block locations.

3. At each block location:
    a. Find the closest point and block support values for conditioning.
    b. Obtain a spatial template configuration formed by the block to be simulated and related conditioning values.
    c. Scan the TI searching for replicates of the above template.
    d. Calculate the spatial cross-support coefficients $L_{i\ldots jk\ldots l}$ using Eq. 33.
    e. Derive the conditional cross-support jpdf $f\left(v_i; z_i^v \middle| \Lambda_0, \Lambda_{i-1}^b\right)$ by first calculating the joint distribution in Eq. 32, then normalizing the distribution in Eq. 30.
    f. Draw a uniform value from $\left[0,1\right]$ to sample z_i^v from the conditional cumulative distribution derived from the above.
    g. Add z_i^v to the simulation grid at block support at location v_i to be used as conditioning value the simulation of a subsequent block.
4. Repeat steps 2 and 3 to generate additional realizations.

3.2.1.2 Sequential Gaussian simulation

The case study in Section 3.3 also applies the sequential Gaussian simulation (SGS) (Isaaks 1990; Journel 1994; Goovaerts 1997). The method assumes that the conditional distribution $f\left(x_i; z_i^p \middle| \Lambda_{i-1}\right)$ is Gaussian, which facilitates the simulation process since its approximation only requires the definition of two parameters, mean and variance. For this reason, the original data is transformed to the Gaussian space typically by a graphical transformation, and at every node location, the method solves a kriging system to obtain the posterior mean and variance. The simulation is performed at the point support scale with subsequent re-blocking procedure to generate block-support models.

3.2.1.3 Mathematical formulation of the simultaneous optimization of mining complexes

The current study uses the simultaneous optimization of mining complexes' model proposed in Goodfellow and Dimitrakopoulos (2016, 2017), which is summarized as follows. In this setting, the mine is discretized into mining blocks indexed in $b \in \mathrm{B}$. The framework considers that each

block has simulated attributes, such as grades and material types, which will denote a stochastic scenario $s \in \mathbb{S}$. The extraction of each block b in the period $t \in T$, incurs a mining cost $MC_{b,t}$, but its extraction can only happen if the set of predecessor $O(b)$ has already been extracted. Once extracted, the material can flow from the mine to a stockpile or a destination such as waste, leach pad or mill (processors $i \in P$). The cost associated with material transportation is given by $TC_{i,a,t}$. The amount of property a in location i, period t and scenario s is quantified in $v_{a,i,t,s}$. Material that flows from the mine to a location, such as tonnages, is indexed in $p \in \wp$, whereas transformations, potentially non-linear ones such as recovery, are indexed in $h \in H$. Thus, $p_{h,t,s}$ denotes the unitary value of selling the material property h, in period t and scenario s. $PC_{i,p,t}$ is the processing cost of treating material property p, in location i at the period t. The set of production targets are represented by $\wp_c$, where deviations are quantified in $d^{\pm}_{i,a,t,s}$ and penalized by the cost $c^{\pm}_{i,a,t}$. The model also incorporates smoothing and sink constraints (Dimitrakopoulos and Ramazan 2004; Saliba and Dimitrakopoulos 2017), where deviations of these targets are quantified in and penalized by $d^{smooth}_{b,t}, d^{sink}_{b,t}$ and $c^{smooth}_{b,t}, c^{sink}_{b,t}$, respectively. Additional sets of constraints as slope, reserve, capacities, destination policy and processing stream constraints are detailed in Goodfellow and Dimitrakopoulos (2016).

There are three types of decision variables in the described model. Extraction sequence $\left(x_{b,t} \in \{0,1\}\right)$ returns 1 if the block b is extracted at the period t, 0 otherwise. Destination decisions $\left(z_{g,j,t} \in \{0,1\}\right)$ define where to send a group of material g to the destination j at the period t. These groups are defined similarly as in Menabde et al. (2007), where pre-defined grade bins are inputted, and the optimizer decides the optimal cut-off grades boundaries. Processing stream decisions $\left(y_{i,j,t,s} \in [0,1]\right)$ define the proportion of material that flows from location i to destination j, in period t and scenario s.

The objective function in Eq. 34 maximizes the value of selling the products in the mineral value chain, while minimizes deviation from production targets.

$$\max \frac{1}{\|\mathbb{S}\|}\left\{\sum_{s\in\mathbb{S}}\sum_{t\in T}\left\{\underbrace{\sum_{i\in P}\sum_{h\in \mathrm{H}} p_{h,t,s} * v_{h,i,t,s}}_{\text{Part I}} - \underbrace{\sum_{i\in P}\sum_{p\in\wp}\left(PC_{i,p,t}+TC_{i,p,t}\right)* v_{p,i,t}}_{\text{Part II}}\right.\right.$$
$$\left.\left.\underbrace{-\sum_{i\in P}\sum_{p\in\wp_c}\left(c^{+}_{i,p,t} * d^{+}_{i,p,t,s} + c^{-}_{i,p,t} * d^{-}_{i,p,t,s}\right)}_{\text{Part III}}\right\}\right\} \underbrace{-\sum_{t\in T}\sum_{b\in \mathrm{B}}\left(MC_{b,t} * x_{b,t} + c^{smooth}_{b,t} * d^{smooth}_{b,t}\right)}_{\text{Part IV}} \tag{34}$$
$$\underbrace{-\sum_{t\in T}\sum_{b\in \mathrm{B}}\sum_{v\in V_b}\left(c^{sink}_{b,t} * d^{sink}_{b,t,v}\right)}_{\text{Part V}}$$

Part I considers the discounted cash flow obtained by selling the products in the value chain. Part II minimizes the processing cost at each processing facility and transportation costs involved. The third and fourth terms are related to the cost of deviating from processing and mining capacities, respectively. Part V and VI minimize the deviation from schedule smoothness and sink rate constraints, respectively. Note that geological risk discounting (Dimitrakopoulos and Ramazan 2004) is applied to all penalty costs associated with production target, i.e

$$c^{\pm}_{i,a,t} = \frac{c^{\pm}_{i,a}}{\left(1+r\right)^{t}} \tag{35}$$

where r is the geological discount rate.

The simultaneous optimization of a mining complex framework presented above is very general, allows for the integration of many sources of uncertainty and can be extremely non-linear. This allowed to the multimillion decision binary variables that the model necessitates solving results in extensive combinatorial optimization. Consequently, solutions via commercial mixed integer programming (MIP) solvers are computationally demanding. For practical cases, metaheuristic algorithms stand as the alternative and have proved to be an efficient solving approach for the stochastic optimization of mines and mining complexes (Lamghari and Dimitrakopoulos 2012, 2014; Lamghari et al. 2014; Goodfellow and Dimitrakopoulos 2016; Montiel and Dimitrakopoulos 2017). They do not prove optimality, but very good solutions can be obtained in a feasible amount of time. The solution approach used in the current paper is from Goodfellow and Dimitrakopoulos (2016, 2017).

3.3 Case Study – applications at a gold mining complex

The first part of the case study is related to the simulation of the gold mine. The deposit covers an area of approximately 4.5 km^2 and a depth of 400 m. The three-dimensional block model block model has more than 500,000 blocks of 10x10x10 m^3. The exploration data available is composed by about 2,300 drillholes of 10 m composite size and spaced at approximately 35 m. A set of 15 high-order simulations are generated directly at the scale of blocks using a training image generated from blasthole data, obtained at every 5m. For comparison, a set of simulations based on the second-order statistics is also generated using one of most traditional methods in industry applications, sequential Gaussian simulation (SGS) (Isaaks 1990; Journel 1994; Goovaerts 1997). Realizations are generated at the point-support and rescaled to block support using a discretization of 25 nodes per block.

3.3.1 Results, comparison and effects of high-order and second-order simulations

First, to provide a common ground for comparison, Fig. 3.2 shows the grade-tonnage curve for both simulation frameworks with comparable overall behaviour. The graph shows very similar proportions regarding tonnages and grades in the whole deposit. Although the metal quantity is very comparable in both cases, how each method connects these elements in space can be very different, especially at the high-grade values, as mentioned earlier in Fig. 3.1. Figure 3.3 displays cross sections of both second-order and high-order realizations of the deposit, where the high-grade zones are highlighted in red circles. It is possible to visualize the effect of the maximal entropy property over the second-order simulations, which is enhanced by the fact the simulation process was performed at the Gaussian space. The grades displayed by the simulations generated with SGS are visually more sparsed than in the high-order simulations. This connectivity can be quantified accordingly to Journel and Alabert (1989), and it is presented in Fig. 3.4. For the connectivity plot, the cut-off applied is 5 g/ton, corresponding to the 99^{th} percentile of the grade distribution, as the focus of the comparison is on the high-grades. In the NE direction, the second-order realizations behave consistently less connected than the high-order ones for all lags. Regarding the NE direction and 45º dip, the difference becomes more pronounced, with a considerable gap between both simulation methods. As the mineralization of high grades drives the mine production schedule, this plays a vital role in the mine complex optimization.

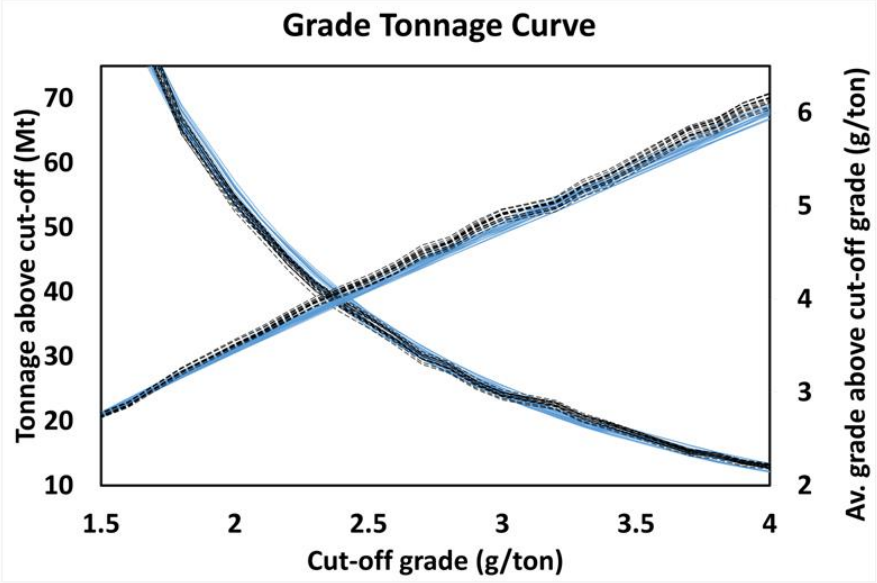

Figure 3.2 – Grade tonnage curve of the gold deposit for SGS and high-order simulations.

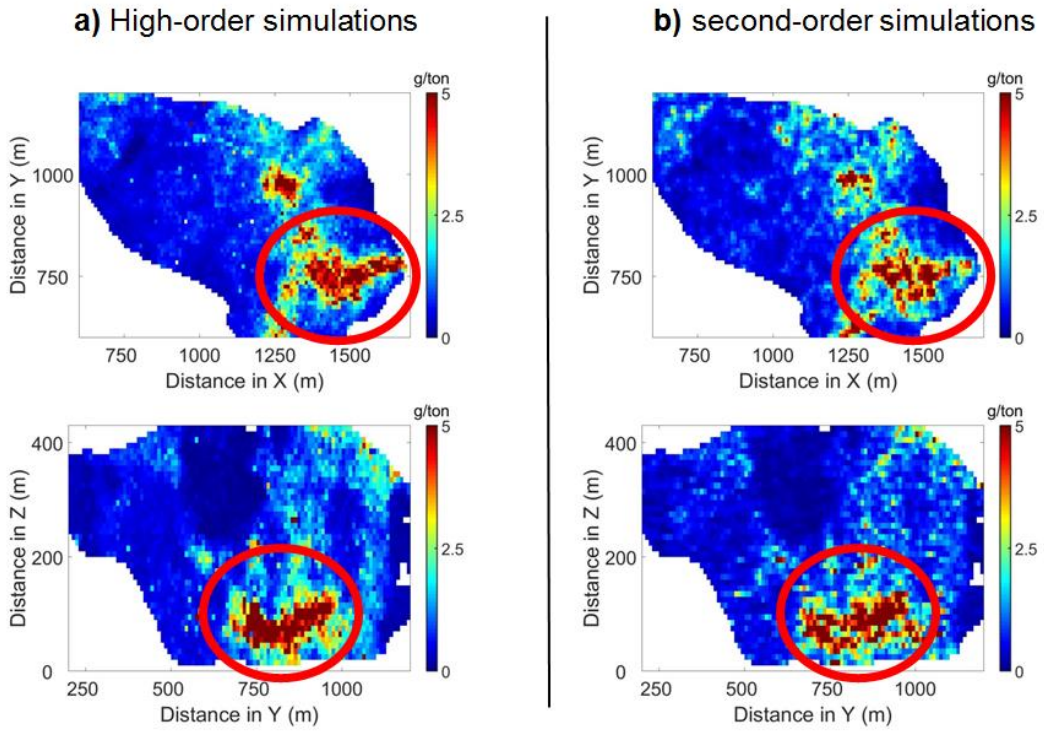

Figure 3.3 - Cross-sections of the simulations highlighting differences in connectivities of high grades: a) high-order simulations; b) SGS simulations.

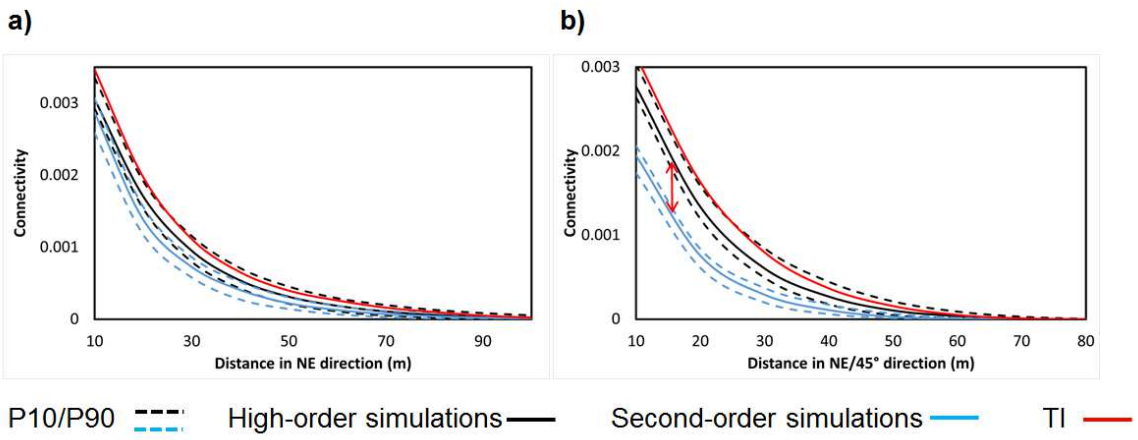

Figure 3.4 – Connectivity of simulated realizations at a) NE direction; b) NE/45º direction

3.3.2 LOM production schedule optimization and forecasting

The simple mining complex version considered in the application consists of a single gold mine, and the following destinations where the material from the mine can flow to a leach pad, a stockpile, a waste dump and a mill circuit. The ore extracted from the mine can flow from the mine to the leach pad or to the mill processing stream to produce gold, the diagram of the mining complex is shown in Fig. 3.5. The critical parameters for the optimization, displayed in Table 3.1, are kept constant in both cases.

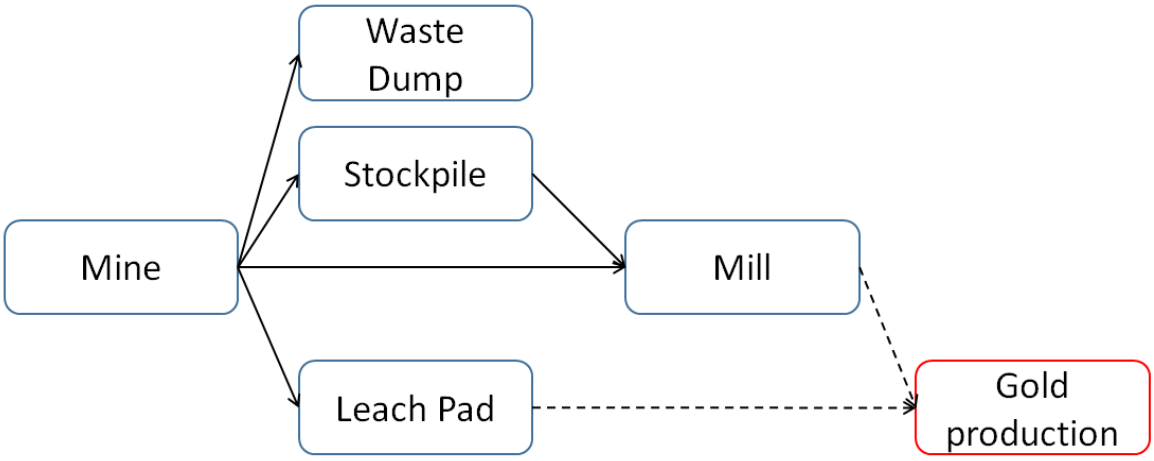

Figure 3.5 – Diagram of the mine complex configuration.

Table 3.1 – Main parameters used in the optimzation

Parameter	**Specification**
Mine capacity	30 Mtpa
Mill capacity	8.25 Mtpa
Leach pad capacity	10 Mtpa
Sink rate	60m / year
Mining radius	60m
Mining cost	1.6$/ton
Milling cost	7.84$/ton
Gold price	1250 $/Oz
Discount rate	10%
Geologic risk discounting	10%

The uncertainty in the materials supplied by the deposit is quantified by the set of simulations generated, and they are inputted into the optimization framework. First, the mining complex is optimized having the simulations generated by the high-order direct block support method, which is referred throughout the remainder of the paper as Case 1. To benchmark the forecasts of life-of-mine (LOM) production schedule obtained, the same mining complex setting is optimized, having the deposit being described by the set of simulations generated by the second-order simulation method. The result of this optimization is referred to as Case 2.

Cases 1 and 2 are optimized and results are discussed below. Cross sections of the LOM production schedules optimized for each case are displayed in Figs. 3.6 and 3.7 along West-East and North-South directions, respectively. The areas with the same colour represent the same period of extraction, and they highlight that the sequences of extraction obtained differ considerably. This is not surprising given the differences in the two simulation methods used, as discussed in previous sections. Cross sections of Case 1 show a clear mining direction controlling the sequence of extraction, highlighted by the red arrow. Note that this direction is approximately the same direction where the difference in connectivity is more evident, recall from Fig. 3.4. The higher continuity of high-grades is driving the schedule towards these more connected ore materials so that they can be processed together.

Figure 3.8 display horizontal sections of the LOM production schedule generated and the differences in of the sequence of extraction are again demonstrated. Additionally, these sections show variations in the extension of the ultimate pit limits (UPL); the red circles highlights how larger the UPL is in Case 2. As second-order simulations methods present high-grade material

more scattered, it is logical that the pits have to be larger to process these elements, resulting in a higher waste extraction as shown in Fig. 3.8a.

These differences are of particular interest since after the optimization part, the process of designing the infrastructure, such as ramps, accesses, equipment placement, facility locations, reduces the flexibility to change the schedule. If the production schedule optimization does not account for more realistic connectivity of high grades, the LOM production schedule cannot pursue the high grades more strategically.

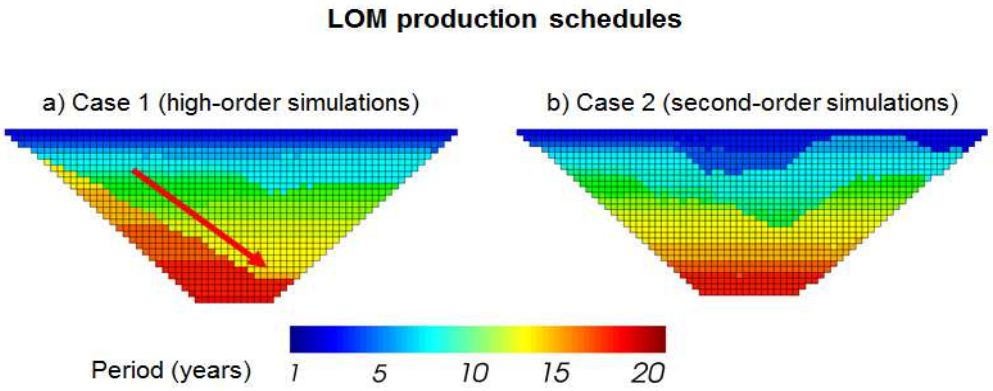

Figure 3.6 – Cross-section of the LOM production schedule (plane East-West) obtained in: a) Case 1 and b) Case 2.

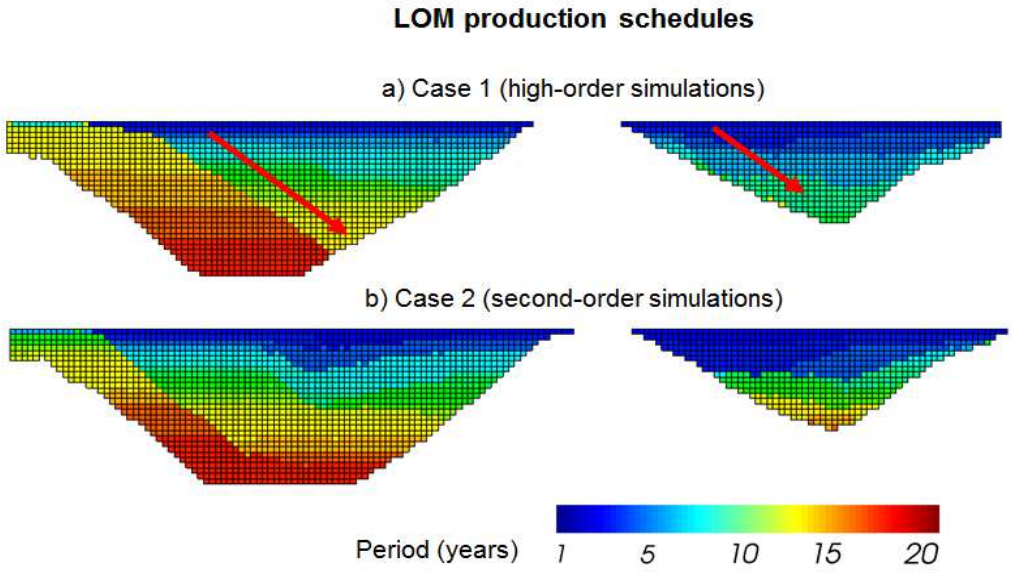

Figure 3.7 – Cross-section of the LOM production schedule (plane North-South) obtained in: a) Case 1 and b) Case 2.

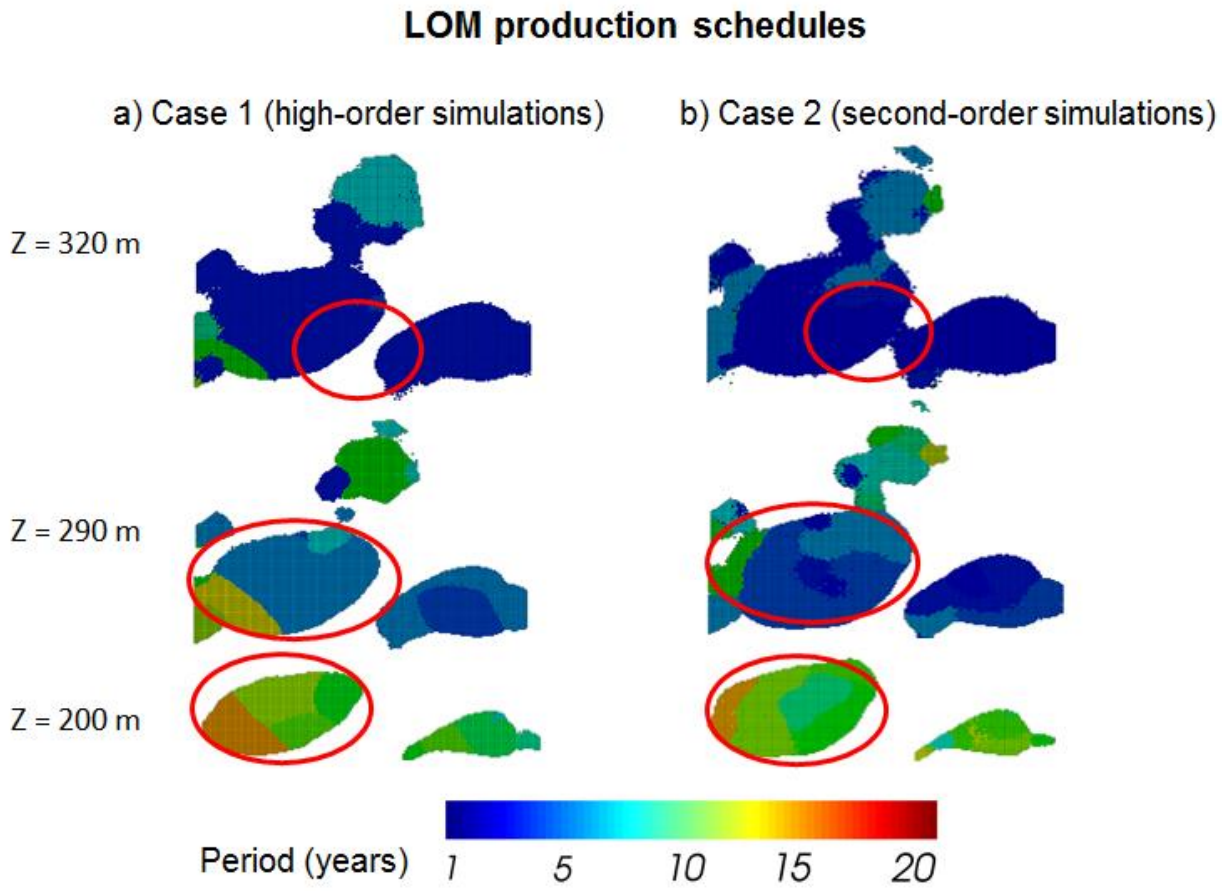

Figure 3.8 –Horizontal sections of the mine production schedule at different elevations for a) Case 1 and b) Case 2.

Regarding production targets and forecasts, Fig. 3.9a shows the total tonnage mined over the LOM and the cumulative strip ratio for both cases. The production schedule obtained in Case 2 mines, in total, 5% more material than Case 1, this difference reaches 8% at the end of the 10th year, to ensure a similar throughput at the mill, Fig. 3.9b. Mining more, in this case, translates to higher waste production, which is quantified by the higher strip ratios presented by Case 2. This can be explained based on the greater spatial disorder (maximal entropy) that second-order, especially Gaussian-based approaches, cause to high-grades. Having the ore blocks less connected in space the optimizer mines more to reach the high-grade values, more sparse, and provide a consistent feed rate at the mill. This contrast in the total tonnage mined leads to the differences in UPL sizes, Fig. 3.8. On the other hand, inputting into the optimizer more realistic connectivities of ore leads the LOM production schedule in Case 1 to be more informed into pursuing high-grades more efficiently.

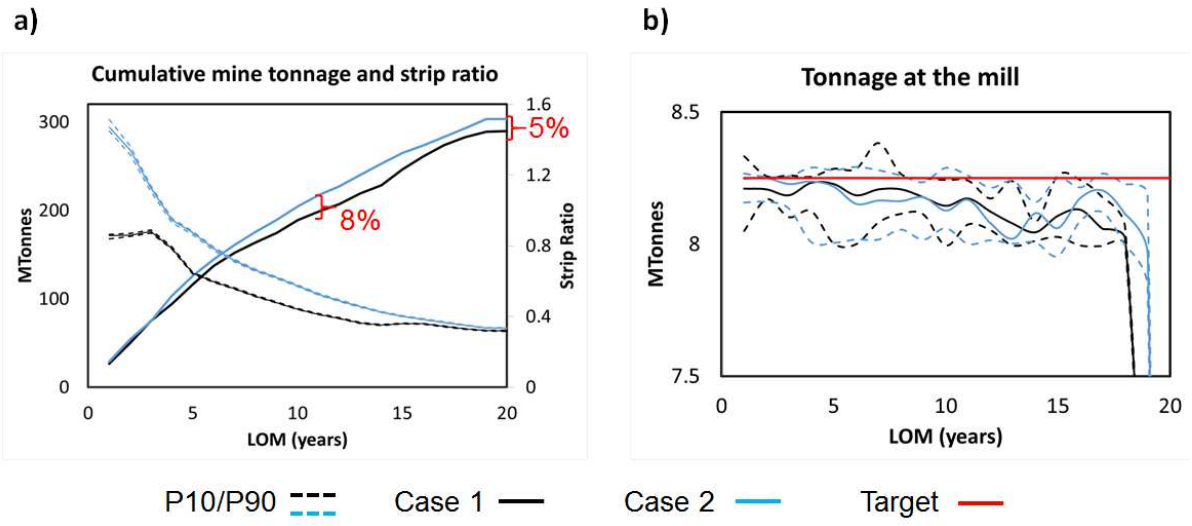

Figure 3.9 – Production target assessments: a) cumulative mine tonnage and strip ratio; b) mill´s throughput.

Although the mill's throughput is kept reasonably constant throughout the LOM in both instances, the dissimilarities regarding metal content are stressed in Fig. 3.10. The Case 1 can feed the mill with a higher head grade for the majority of the LOM, as shown in Fig. 3.10a. As the optimizer sees high grades better connected, it is easier to bring their extraction to the same period so they can be processed together. These richer materials mined are processed together increasing the average feed grade at the mill, consequently recovering more ounces earlier, as shown in Fig. 3.10b. Case 1 has an ounces profile consistently higher for the first 17 years; this difference reaches 7% after the 10th year. Case 2 produces, after the 20th year, 2% more gold, but this is not significant due to the effect of discounting and the time value of money. Recovering more ounces sooner brings more cash flow earlier to the operation which positively impacts the NPV. Summing the joint effects of meeting the targets, mining less waste, and producing more gold ounces at earlier stages results in a considerable increase in NPV, as shown in Fig. 3.10c. By producing more metal for less waste, the LOM production schedule obtained in Case 1 generates in total 5% more NPV than Case 2, and 16% more in the initial ten years. The difference is substantial and greatly appreciated especially at early stages of the development of the mine.

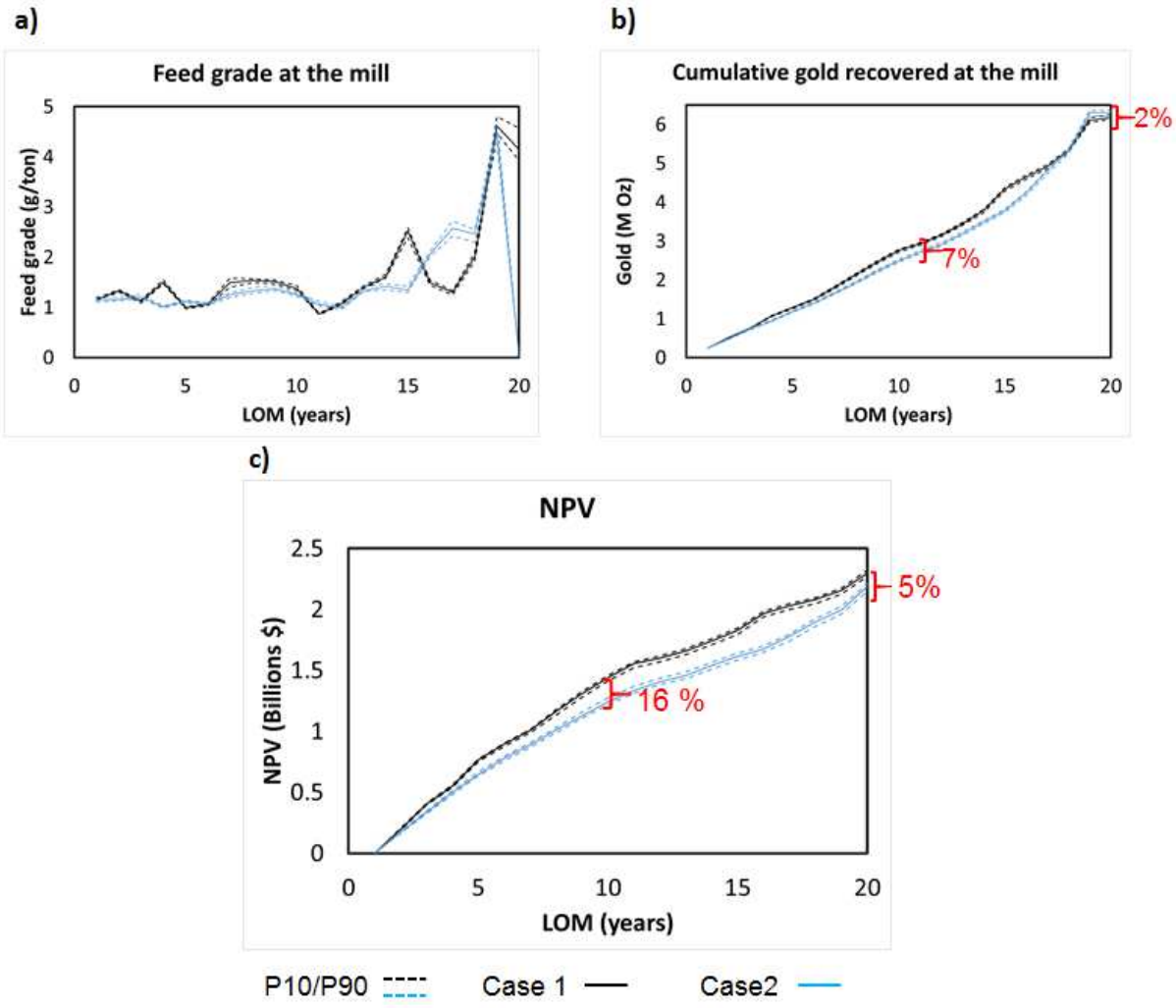

Figure 3.10 – Risk analysis of production forecasts for a) head grade at the mill; b) cumulative gold recovered at the mill and c) NPV assessment.

3.4 Conclusions

This paper investigates the effects of high-order simulations of a deposit in the simultaneous stochastic optimization of a gold mining complex. The high-order simulations are generated directly at the block-support scale and are inputted in the simultaneous optimization (Case 1). The LOM production schedule generated is benchmarked against a case where the stochastic realizations of the orebody are generated through the use of a conventional second-order simulation method, SGS (Case 2). The geological realizations from both methods present comparable proportions of tonnages and grades, but very different spatial connectivity of high-grades. Frameworks based on the second-order statistics, in particular Gaussian-based, maximize

the spatial disorder of the generated realizations preventing the reproduction of the connectivity of high-grades.

In this study, the high-order simulations present a higher degree of continuity of high-grades, which is notably more pronounced at the NE/45º direction, when compared to the second-order simulations. This information is incorporated into the simultaneous stochastic optimization framework driving the sequence of extraction more smartly favouring this direction. The direct consequence of the above is the Case 1 scheduling sequences with more high-grade material, which allows the optimization to process them together increasing the mill's head grade. The result is a higher ounce profile being produced earlier, up to 7% more gold being recovered by the end of the year 10. Note that this is achieved while mining less waste, the strip ratio of Case 1 is consistently below Case 2. In its turn, the Case 2 generates a pit 5% larger to provide a similar mill's throughput throughout the LOM. The combined effect of producing more metal while mining less waste in this case study is the increase in NPV by 5 to 16% than the assessment obtained in Case 2. These findings corroborate that the choice of a simulation method matters and that the simultaneous stochastic optimization of mining complex can profit from the benefits of incorporating simulations, that can reproduce multi-point connectivity of high-grades, into the optimization.

Chapter - 4

Conclusions

4.1 – General conclusions

The present work shows that the simultaneous stochastic optimization of mining complex can profit by incorporating simulations that better capture multi-point connectivity of high-grades of an underlying mineral deposit. Current state-state-of-the art simulations methods are capable of modelling spatially distributed geologic non-Gaussian geologic attributes with complex and non-linear geometries. However, they output realizations at the point-support scale, requiring post-process to generate engineering block model to represent the orebody. Massive mineral deposits represented by several million mining blocks are computationally cumbersome to not only generate the models but to handle simulated files and re-block realizations into adequate mining block sizes. This observation motivated this thesis to extend the high-order simulation method to generate stochastic realizations of spatially distributed phenomena directly at block-support scale, which improves the computational efficiency of existing methods. Data handling is facilitated by the elimination of the re-blocking post-processing step. The stochastic realizations generated from this framework are inputted to the simultaneous stochastic optimization of a gold mining complex optimization, where the influence of the high-order simulations on the life-of-mine (LOM) production schedule is evaluated and highlighted. The case study illustrates the benefits of using methods that reproduce more realistically the mineralization of high-grades and presents a possibility to generate more informed schedules, driven by the spatial structures and continuity of high grade blocks.

This thesis presents a high-order direct block simulation method that generates realizations at the block-support scale conditional to the available drillhole data, at point-support. Following the sequential simulation approach, the method estimates at every block location a cross-support joint probability density function conditional to values at different support scale. It allows sampling a value directly at the block-support. The method uses a training image at point-support, which is up-scaled to represent block-support and assist with the calculation of spatial cumulants, as needed. At each block location, a spatial template able to obtain conditioning values in different supports is defined, and the TI in both support sizes acts as a database for

replicates to the calculation of the spatial cumulants. The high-order aspect of the framework ensures that simulated realizations reproduce complex and non-linear geological spatial geometries of the attribute of interest directly at block scale. The method is tested in a controlled environment showing that the realizations can reasonably reproduce the most important spatial structures observed in the exhaustive images. The approach is applied to a gold deposit where realizations show good compliance with the spatial statistics of the data up to the fourth-order cumulants. The runtime of generating one realization in this application shows a reduction by a factor of 5 when compared to the point-support version of the algorithm, without considering reblocking.

The simulations of the gold deposit generated are subsequently used in a case study that considers the simultaneous stochastic optimization of a mining complex, comprising of one mine, a waste dump, a mill and a leach pad, and gold is the single product of interest. The stochastic realizations of the deposit, quantifying the uncertainty and variability, and reproducing the multi-point connectivity of high-grade, are used as inputs in this simultaneous optimization framework. Results of the LOM production schedule obtained (Case 1) is benchmarked to a similar setting but having the deposit characterized by a conventional second-order sequential (Gaussian) simulation method (Case 2). First, the application compares the intricacies of both simulation methods applied, and findings show that even though displaying very similar overall proportion of tonnages and grades, the manner in which each method connects the ore is very different. The study shows that the connectivity of high-grade effectively plays a role by visually driving the sequence of extraction towards the direction where this difference in connectivity pronounced between realizations from both methods. This more informed mining strategy impacts positively the LOM production schedule, which can capitalize on this more realistic modelling, and provides a series of benefits. First, the comparison shows that the LOM production of Case 1 produces more ounces earlier in the LOM than Case 2, 7% more gold is recovered by the end of period 10. It is important to mention that more metal is obtained while less waste is required to mine. The resulting strip ratio is consistently lower than Case 2, which mines more material (5% larger pit) to ensure a similar ore tonnage feeding the mill. The combined effect of these results is an increase of about 5 to 16% net present value compared to Case 2. This highlights that generating more realistic simulations is a key aspect in mine

planning and its integration into the simultaneous optimization of mining complex can enhance even more the value of stochastic solutions.

4.2 – Recommendations for future work

Faster algorithms are still necessary as computational efficiency is still the limit for the industry to adopt more robust methods able to describe more complex geological spatial patterns. Thus, parallelization and the use of GPU computing are an option to improve the time required to model these attributes. Future work in high-order simulations can aim attention at extending the high-order direct block-support approach to perform simulations of correlated elements. Most commonly more than one element is of interest in a mining complex, in which these mineralized attributes are correlated somehow, where decorrelation based on high-order statistics from the data can be further studied. A method able to generate jointly multiple simulations based on high-order statistics directly at block-support has a great potential to improve computational efficiency and data handling.

Additional efforts can focus on generating TI consistent with the high-order relations in the available data. High-order cumulants are dependent on lower orders, which can be easily obtained from the data, this knowledge can be explored in conditioning the training image to the data, thus enhancing the data-driven property of the generated realizations. Today's practices of generating training images are sometimes subjective such as a geologic interpretation (categorical attributes) or require other sources of information such the use of previously mined areas or from blasthole data (continuous attributes).

Finally, having high-order simulated of correlated elements, further study can investigate their influence in the optimization of a more sophisticated mining complex.

References

Alabert F (1987) Stochastic imaging of spatial distributions using hard and soft information. MSc Thesis, University of Queensland, Brisbane, Qld, Australia

Albor F, and Dimitrakopoulos R (2009) Stochastic mine design optimisation based on simulated annealing: pit limits, production schedules, multiple orebody scenarios and sensitivity analysis. Min. Technol. IMM Trans. Sect. A 118(2):79–90. doi: 10.1179/037178409X12541250836860

Arpat GB, and Caers J (2007) Conditional simulation with patterns. Math. Geol. 39(2):177–203. doi: 10.1007/s11004-006-9075-3

Arthur D, and Vassilvitskii S (2007) K-means++: The advantages of careful seeding. In: Proceedings of the Eighteenth Annual ACM-SIAM Symposium on Discrete Algorithms. Society for Industrial and Applied Mathematics, Philadelphia, PA, USA, pp 1027–1035

Benndorf J, and Dimitrakopoulos R (2007) New efficient methods for conditional simulation of large orebodies. In: Dimitrakopoulos R (ed) Orebody Modelling and Strategic Mine Planning. AusIMM, Spectrum Series 14, Carlton, Vic, pp 61–67

Birge J, and Louveaux F (1997) Introduction to stochastic programming. Springer Ser Oper Res. 421. doi: 10.1057/palgrave.jors.2600031

Boucher A (2009) Considering complex training images with search tree partitioning. Comput. Geosci. 35(6):1151–1158. doi: 10.1016/j.cageo.2008.03.011

Boucher A, and Dimitrakopoulos R (2009) Block simulation of multiple correlated variables. Math. Geosci. 41(2):215–237. doi: 10.1007/s11004-008-9178-0

Chanda E (2007) Network linear programming optimisation of an Integrated mining and metallurgical complex. In: Dimitrakopoulos R (ed) Orebody Modelling and Strategic Mine Planning. AusIMM, Spectrum Series 14, pp 149–155

Chatterjee S, Dimitrakopoulos R, and Mustapha H (2012) Dimensional reduction of pattern-based simulation using wavelet analysis. Math. Geosci. 44(3):343–374. doi: 10.1007/s11004-012-9387-4

Chatterjee S, Mustapha H, and Dimitrakopoulos R (2016) Fast wavelet-based stochastic

simulation using training images. Comput. Geosci. 20(3):399–420. doi: 10.1007/s10596-015-9482-y

Dagdelen K, and Traore I (2014) Open pit transition depth determination through global analysis of open pit and underground mine production scheduling. In: Dimitrakopoulos R (ed) Orebody modelling and strategic mine planning. AusIMM, Spectrum Series 14, Melbourne, pp 195–200

David M (1977) Geostatistical ore reserve estimation. Elsevier, Amsterdam

David M (1988) Handbook of applied advanced geostatistical ore reserve estimation. Elsevier, Amsterdam

Davis MW (1987) Production of conditional simulations via the LU triangular decomposition of the covariance matrix. Math. Geol. 19(2):91–98. doi: 10.1007/BF00898189

de Boor C (1978) A practical guide to splines. Springer-Verlag, Berlin

de Carvalho JP, Dimitrakopoulos R, and Minniakhmetov I (2018) High-order block support spatial simulation and application at a gold deposit. Math. Geosci. (Submitted):

Del Castillo MF (2018) Dynamic simultaneous optimization of mineral value chains under resource uncertainty. PhD thesis, McGill University, Canada

Del Castillo MF, and Dimitrakopoulos R (2016) A multivariate destination policy for geometallurgical variables in mineral value chains using coalition-formation clustering. Resour Policy. 50. 322–332. doi: 10.1016/J.RESOURPOL.2016.10.003

Desbarats AJ, and Dimitrakopoulos R (2000) Geostatistical simulation of regionalized pore-size distributions using min/max autocorrelation factors. Math. Geol. 32(8):919–942. doi: 10.1023/A:1007570402430

Deutsch C V., and Wen XH (2000) Integrating large-scale soft data by simulated annealing and probability constraints. Math. Geol. 32(1):49–67. doi: 10.1023/A:1007502817679

Deutsch C V, and Cockerham PW (1994) Practical considerations in the application of simulated annealing to stochastic simulation. Math. Geol. 26(1):67–82. doi: 10.1007/BF02065876

Dimitrakopoulos R (2011) Stochastic optimization for strategic mine planning: A decade of developments. J. Min. Sci. 47(2):138–150. doi: 10.1134/S1062739147020018

Dimitrakopoulos R (1996) Stochastic methods for petroleum reservoir characterization and product forecasting. J Japanese Assoc Pet Technol. 61

Dimitrakopoulos R, Farrelly CT, and Godoy M (2002a) Moving forward from traditional optimization: grade uncertainty and risk effects in open-pit design. Min. Technol. 111(1):82–88. doi: 10.1179/mnt.2002.111.1.82

Dimitrakopoulos R, Farrelly CT, and Godoy M (2002b) Moving forward from traditional optimization: grade uncertainty and risk effects in open-pit design. Min. Technol. 111(1):82–88. doi: 10.1179/mnt.2002.111.1.82

Dimitrakopoulos R, and Godoy M (2014) Grade control based on economic ore/waste classification functions and stochastic simulations: examples, comparisons and applications. Min. Technol. 123(2):90–106. doi: 10.1179/1743286314Y.0000000062

Dimitrakopoulos R, and Luo X (2004) Generalized sequential Gaussian simulation on group size v and screen-effect approximations for large field simulations. Math. Geol. 36(5):567–590. doi: 10.1023/B:MATG.0000037737.11615.df

Dimitrakopoulos R, Mustapha H, and Gloaguen E (2010) High-order statistics of spatial random fields: exploring spatial cumulants for modeling complex non-Gaussian and non-linear phenomena. Math. Geosci. 42(1):65–99. doi: 10.1007/s11004-009-9258-9

Dimitrakopoulos R, and Ramazan S (2004) Uncertainty-based production scheduling in open pit mining. SME Annu. Meet. 316(03):106–112

Dowd P (1994) Risk assessment in reserve estimation and open-pit planning. Trans. Inst. Min. Metall. (January):148–154. doi: 10.1016/0148-9062(95)97056-O

Dowd PA (1997) Risk in minerals projects: analysis, perception and management. Trans Inst Min Metall Sect a-Mining Ind. 106. 9–18

Emery X (2009) Change-of-support models and computer programs for direct block-support simulation. Comput. Geosci. 35(10):2047–2056. doi: https://doi.org/10.1016/j.cageo.2008.12.010

Farmer IW (2016) Stochastic mining supply chain optimization: A study of integrated capacity decisions and pushback design under uncertainty. McGill University, Montreal, QC, Canada

Froidevaux R (1992) Probability field simulation. In: Soares A (ed) Geostatistics Tróia ’92: Volume 1. Springer Netherlands, Dordrecht, pp 73–83

Geman S, and Geman D (1984) Stochastic relaxation, Gibbs distributions, and the Bayesian restoration of images. Pattern Anal. Mach. Intell. IEEE Trans. PAMI-6(6):721–741. doi: 10.1109/TPAMI.1984.4767596

Godoy M (2003) The effective management of geological risk in long-term production scheduling of open pit mines. Ph.D. Thesis, University of Queensland, Brisbane, Qld, Australia

Gómez-Hernández JJ, and Wen XH (1998) To be or not to be multi-Gaussian? A reflection on stochastic hydrogeology. Adv. Water Resour. 21(1):47–61. doi: 10.1016/S0309-1708(96)00031-0

Goodfellow R, Albor Consuegra F, Dimitrakopoulos R, and Lloyd T (2012) Quantifying multi-element and volumetric uncertainty, Coleman McCreedy deposit, Ontario, Canada. Comput Geosci. 42. 71–78. doi: 10.1016/j.cageo.2012.02.018

Goodfellow R, and Dimitrakopoulos R (2016) Global optimization of open pit mining complexes with uncertainty. Appl Soft Comput J. 40. 292–304. doi: 10.1016/j.asoc.2015.11.038

Goodfellow R, and Dimitrakopoulos R (2017) Simultaneous stochastic optimization of mining complexes and mineral value chains. Math. Geosci. 49(3):341–360. doi: 10.1007/s11004-017-9680-3

Goovaerts P (1997) Geostatistics for natural resources evaluation. Oxford University Press, New York

Groeneveld B, Topal E, and Leenders B (2010) A new methodology for flexible mine design. In: Dimitrakopoulos R (ed) Orebody Modelling and Strategic Mine Planning. AusIMM, Spectrum Series 17, pp 113–122

Guardiano FB, and Srivastava RM (1993) Multivariate geostatistics: beyond bivariate moments. In: Soares A (ed) Geostatistics Tróia ’92: Volume 1. Springer Netherlands, Dordrecht, pp 133–144

Hoerger S, Hoffman L, and Seymour F (1999) Mine planning at Newmont’s Nevada operations.

Min. Eng. 51(10):26–30

Huang T, Lu DT, Li X, and Wang L (2013) GPU-based SNESIM implementation for multiple-point statistical simulation. Comput Geosci. 54. 75–87. doi: 10.1016/j.cageo.2012.11.022

Isaaks EH (1990) The application of Monte Carlo methods to the analysis of spatially correlated data. Ph.D. Thesis, Stanford University, Stanford, Ca, United States

Isaaks EH, and Srivastava RM (1989) Applied geostatistics. Oxford University Press

Johnson ME (1987) Multivariate statistical simulation. John Wiley & Sons, Inc., Hoboken, NJ, USA

Journel AG (1974) Geostatistics for conditional simulation of ore bodies. Econ Geol. doi: 10.2113/gsecongeo.69.5.673

Journel AG (2007) Roadblocks to the evaluation of ore reserves - The simulation overpass and putting more geology into numerical models of deposits. In: Dimitrakopoulos R (ed) Orebody Modelling and Strategic Mine Planning. Australasian Institute of Mining and Metallurgy, pp 29–32

Journel AG (2018) Roadblocks to the evaluation of ore reserves - the simulation overpass and putting more geology into numerical models of deposits. In: Dimitrakopoulos R (ed) Advances in Applied Strategic Mine Planning. Springer, Heidelberg, pp 47–55

Journel AG (2005) Beyond covariance: the advent of multiple-point geostatistics. In: Leuangthong O, Deutsch C V. (eds) Geostatistics Banff 2004, Quantitative Geology and Geostatistics, vol 14. Springer, Dordrecht, pp 225–233

Journel AG (1994) Modeling uncertainty: some conceptual thoughts. In: Dimitrakopoulos R (ed) Geostatistics for the Next Century. Springer, Dordrecht, pp 30–43

Journel AG, and Alabert F (1989) Non-gaussian data expansion in the earth sciences. Terra Nov. 1(2):123–134. doi: 10.1111/j.1365-3121.1989.tb00344.x

Journel AG, and Deutsch C V. (1993) Entropy and spatial disorder. Math. Geol. 25(3):329–355. doi: 10.1007/BF00901422

Journel AG, and Huijbregts CJ (1978) Mining geostatistics. Blackburn Press, New York

Kennedy J, and Eberhart R (1995) Particle swarm optimization. In: Proceedings of IEEE International Conference on Neural Networks. IEEE, pp 1942–1948

Kirkpatrick S, Gelatt CD, and Vecchi MP (1983) Optimization by simulated annealing. Science (80-.). 220(4598):671 LP-680

Kumar A, and Dimitrakopoulos R (2017) Introducing geometallurgical constraints into the simultaneous stochastic optimization of mining complexes: Application at a copper-gold mining complex. In: Dagdelen K (ed) Proceedings of 38th International Symposium on the Application of Computers and Operations Research in the Mineral Industry. APCOM, pp 6-7-6–14

Lamghari A, and Dimitrakopoulos R (2014) Progressive hedging applied as a metaheuristic to schedule production in open-pit mines accounting for reserve uncertainty. Eur. J. Oper. Res. 24(3):843–855. doi: 10.1016/j.ejor.2016.03.007

Lamghari A, and Dimitrakopoulos R (2012) A diversified Tabu search approach for the open-pit mine production scheduling problem with metal uncertainty. Eur. J. Oper. Res. 222(3):642–652. doi: 10.1016/j.ejor.2012.05.029

Lamghari A, Dimitrakopoulos R, and Ferland JA (2014) A variable neighbourhood descent algorithm for the open-pit mine production scheduling problem with metal uncertainty. J. Oper. Res. Soc. 65(9):1305–1314. doi: 10.1057/jors.2013.81

Lebedev NN (1965) Special functions and their applications. Prentice-Hall Inc., New York

Leite A, and Dimitrakopoulos R (2007) Stochastic optimisation model for open pit mine planning: application and risk analysis at copper deposit. Min. Technol. 116(3):109–118. doi: 10.1179/174328607X228848

Li X, Mariethoz G, Lu DT, and Linde N (2016) Patch-based iterative conditional geostatistical simulation using graph cuts. Water Resour. Res. 52(8):6297–6320. doi: 10.1002/2015WR018378

Maharaja A (2004) Hierarchical simulation of multiple facies reservoir using multiple-point geostatistics. M.Sc. Thesis, Stanford University, Stanford, CA

Mariethoz G, and Caers J (2014) Multiple-point geostatistics: Stochastic modeling with training

images. Hoboken: Wiley

Mariethoz G, Renard P, and Straubhaar J (2010) The direct sampling method to perform multiple-point geostatistical simulations. Water Resour. Res. 46(11):1–14. doi: 10.1029/2008WR007621

Menabde M, Froyland G, Stone P, and Yeates GA (2007) Mining schedule optimisation for conditionally simulated orebodies. Orebody Model Strateg Mine Plan. 14. 379–383

Minniakhmetov I, and Dimitrakopoulos R (2017a) Joint high-order simulation of spatially correlated variables using high-order spatial statistics. Math. Geosci. 49(1):39–66. doi: 10.1007/s11004-016-9662-x

Minniakhmetov I, and Dimitrakopoulos R (2017b) A high-order, data-driven framework for joint simulation of categorical variables. In: Gómez-Hernández JJ, Rodrigo-Ilarri J, Rodrigo-Clavero ME, et al. (eds) Geostatistics Valencia 2016. Springer International Publishing, Cham, pp 287–301

Minniakhmetov I, Dimitrakopoulos R, and Godoy M (2018) High-order spatial simulation using Legendre-like orthogonal splines. Math Geosci. doi: 10.1007/s11004-018-9741-2

Montiel L, and Dimitrakopoulos R (2013) Stochastic mine production scheduling with multiple processes: Application at Escondida Norte, Chile. J. Min. Sci. 49(4):583–597. doi: 10.1134/S1062739149040096

Montiel L, and Dimitrakopoulos R (2018) Simultaneous stochastic optimization of production scheduling at Twin Creeks Mining Complex , Nevada. Min. Eng. 70(12):12–20

Montiel L, and Dimitrakopoulos R (2015) Optimizing mining complexes with multiple processing and transportation alternatives: An uncertainty-based approach. Eur. J. Oper. Res. 247(1):166–178. doi: 10.1016/j.ejor.2015.05.002

Montiel L, and Dimitrakopoulos R (2017) A heuristic approach for the stochastic optimization of mine production schedules. J. Heuristics 23(5):397–415. doi: 10.1007/s10732-017-9349-6

Montiel L, Dimitrakopoulos R, and Kawahata K (2016) Globally optimising open-pit and underground mining operations under geological uncertainty. Min. Technol. 125(1):2–14. doi: 10.1179/1743286315Y.0000000027

Mustapha H, Chatterjee S, and Dimitrakopoulos R (2014) CDFSIM: efficient stochastic simulation through decomposition of cumulative distribution functions of transformed spatial patterns. Math. Geosci. 46(1):95–123. doi: 10.1007/s11004-013-9490-1

Mustapha H, and Dimitrakopoulos R (2010a) High-order stochastic simulation of complex spatially distributed natural phenomena. Math. Geosci. 42(5):457–485. doi: 10.1007/s11004-010-9291-8

Mustapha H, and Dimitrakopoulos R (2011) HOSIM: A high-order stochastic simulation algorithm for generating three-dimensional complex geological patterns. Comput. Geosci. 37(9):1242–1253. doi: 10.1016/j.cageo.2010.09.007

Mustapha H, and Dimitrakopoulos R (2010b) A new approach for geological pattern recognition using high-order spatial cumulants. Comput. Geosci. 36(3):313–334. doi: 10.1016/j.cageo.2009.04.015

Ortiz JM, and Peredo O (2010) Multiple point geostatistical simulation with simulated annealing: Implementation using speculative parallel computing. In: Atkinson PM, Lloyd CD (eds) geoENV VII -- Geostatistics for Environmental Applications. Springer Netherlands, Dordrecht, pp 383–394

Osterholt V, and Dimitrakopoulos R (2007) Simulation of wireframes and geometric features with multiple-point techniques: application at Yandi iron ore deposit. In: Dimitrakopoulos R (ed) Orebody Modelling and Strategic Mine Planning. AusIMM Spectrum Series, pp 51–60

Peredo O, and Ortiz JM (2011) Parallel implementation of simulated annealing to reproduce multiple-point statistics. Comput. Geosci. 37(8):1110–1121. doi: 10.1016/j.cageo.2010.10.015

Pimentel BS, Mateus GR, and Almeida FA (2010) Mathematical models for optimizing the global mining supply chain. In: Nag B (ed) Intelligent Systems in Operations: Methods, Models and Applications in the Supply Chain. IGI Global, pp 133–163

Qureshi SE, and Dimitrakopoulos RG (2005) Comparison of stochastic simulation algorithms in mapping spaces of uncertainty of non-linear transfer functions. In: Leuangthong O, Deutsch C V. (eds) Geostatistics Banff 2004, Quantitative Geology and Geostatistics, vol 14. Springer, Dordrecht, pp 959–968

Ramazan S, and Dimitrakopoulos R (2013) Production scheduling with uncertain supply: A new solution to the open pit mining problem. Optim. Eng. 14(2):361–380. doi: 10.1007/s11081-012-9186-2

Ravenscroft PJ (1992) Risk analysis for mine scheduling by conditional simulation. Trans. Inst. Min. Met. (Sec. A Min. Ind. 101

Remy N, Boucher A, and Wu J (2009) Applied geostatistics with SGeMS: a user's guide. Cambridge University Press, Cambridge

Renard P, and Allard D (2013) Connectivity metrics for subsurface flow and transport. Adv Water Resour. doi: 10.1016/j.advwatres.2011.12.001

Rezaee H, Mariethoz G, Koneshloo M, and Asghari O (2013) Multiple-point geostatistical simulation using the bunch-pasting direct sampling method. Comput. Geosci. 54(September 2017):293–308. doi: 10.1016/j.cageo.2013.01.020

Rocchi L, Carter P, and Stone P (2011) Sequence optimization in longwall coal mining. J. Min. Sci. 47(2):151–157. doi: 10.1134/S106273914702002X

Rossi ME, and Deutsch C V. (2014) Mineral resource estimation. Springer Netherlands

Saliba Z, and Dimitrakopoulos R (2017) Simultaneous stochastic optimization of an open pit gold mine complex with supply and market uncertainty. In: Dimitrakopoulos R (ed) COSMO Research Report No 11, Vol . 1. COSMO - Stochastic Mine Planning Laboratory, pp 173–200

Soares A (2001) Direct sequential simulation and cosimulation. Math. Geol. 33(8):911–926. doi: 10.1023/A:1012246006212

Stone P, Froyland G, Menabde M, et al (2007) Blasor–blended iron ore mine planning optimization at Yandi, Western Australia. In: Dimitrakopoulos R (ed) Orebody modelling and strategic mine planning: Uncertainty and risk management models. AusIMM, Spectrum Series 14, pp 133–136

Straubhaar J, Renard P, Mariethoz G, et al (2011) An improved parallel multiple-point algorithm using a list approach. Math. Geosci. 43(3):305–328. doi: 10.1007/s11004-011-9328-7

Strebelle S (2002) Conditional simulation of complex geological structures using multiple-point

statistics. Math. Geol. 34(1):1–21. doi: 10.1023/A:1014009426274

Strebelle S, and Cavelius C (2014) Solving speed and memory issues in multiple-point statistics simulation program SNESIM. Math. Geosci. 46(2):171–186. doi: 10.1007/s11004-013-9489-7

Stuart A, and Ord JK (1987) Kendall's advanced theory of statistics

Switzer P, and Green AA (1984) Min/max autocorrelation factors for multivariate spatial imaging: Technical Report No. 6. 14

Topal E, and Ramazan S (2012) Strategic mine planning model using network flow model and real case application. Int. J. Mining, Reclam. Environ. 26(1):29–37. doi: 10.1080/17480930.2011.600827

Urbaez E, and Dagdelen K (1999) Implementation of linear programming model for optimum open pit production scheduling problem. In: Transactions of the Society of Mining, Metallurgy and Exploration, Inc. pp 1968–1974

Vallée M (2000) Mineral resource + engineering, economic and legal feasibility = ore reserve. Can Min Metall Soc Bull. 93. 53–61

Wei Y, Wang G, and Yang P (2013) Legendre-like orthogonal basis for spline space. CAD Comput. Aided Des. 45(2):85–92. doi: 10.1016/j.cad.2012.07.011

Whittle G (2007) Global asset optimization. In: Dimitrakopoulos R (ed) Orebody Modelling and Strategic Mine Planning: Uncertainty and Risk Management Models. AusIMM, Spectrum Series 14, Carlton, Vic, pp 331–336

Whittle J (2010) The global optimiser works – what next ? In: Dimitrakopoulos R (ed) Advance in Applied Orebody Modelling and Strategic Mine Planning. AusIMM, Spectrum Series, 17, pp 3–5

Wu J, Zhang T, and Journel A (2008) Fast FILTERSIM simulation with score-based distance. Math. Geosci. 40(7):773–788. doi: 10.1007/s11004-008-9157-5

Yao L, Dimitrakopoulos R, and Gamache M (2018) A new computational model of high-order stochastic simulation based on spatial Legendre moments. Math Geosci. doi: 10.1007/s11004-018-9744-z

Zhang J, and Dimitrakopoulos RG (2017) A dynamic-material-value-based decomposition method for optimizing a mineral value chain with uncertainty. Eur. J. Oper. Res. 258(2):617–625. doi: 10.1016/j.ejor.2016.08.071

Zhang T, Gelman A, and Laronga R (2017) Structure- and texture-based fullbore image reconstruction. Math. Geosci. 49(2):195–215. doi: 10.1007/s11004-016-9649-7

Zhang T, Switzer P, and Journel A (2006) Filter-based classification of training image patterns for spatial simulation. Math. Geol. 38(1):63–80. doi: 10.1007/s11004-005-9004-x

Zuckerberg M, Stone P, Pasyar R, and Mader E (2007) Joint ore extraction and in-pit dumping optimisation. In: Dimitrakopoulos R (ed) Orebody Modelling and Strategic Mine Planning. AusIMM, Spectrum Series 14, pp 137–140

Zuckerberg M, van der Riet J, Malajczuk W, and Stone P (2011) Optimal life-of-mine scheduling for a bauxite mine. J. Min. Sci. 47(2):158–165. doi: 10.1134/S1062739147020031